https://doi.org/10.5607/en21035
Exp Neurobiol. 2022 Jun;31(3):173-195.
pISSN 1226-2560 • eISSN 2093-8144

Original Article

Experimental Neurobiology

Astrocyte-targeted Overproduction of IL-10 Reduces Neurodegeneration after TBI

Mahsa Shanaki-Bavarsad[1,2], Beatriz Almolda[1,2*], Berta González[1,2] and Bernardo Castellano[1,2]
[1]Institute of Neurosciences, Universitat Autònoma de Barcelona, [2]Department of Cell Biology, Physiology and Immunology, Universitat Autònoma de Barcelona, Bellaterra, 08193 Barcelona, Spain

Traumatic brain injury is the greatest cause of disability and death in young adults in the developed world. The outcome for a TBI patient is determined by the severity of the injury, not only from the initial insult but, especially, as a product of the secondary injury. It is proposed that this secondary injury is directly linked to neuro-inflammation, with the production of pro-inflammatory mediators, activation of resident glial cells and infiltration of peripheral immune cells. In this context, anti-inflammatory treatments are one of the most promising therapies to dampen the inflammatory response associated with TBI and to reduce secondary injury. In this sense, the main objective of the present study is to elucidate the effect of local production of IL-10 in the neurological outcome after TBI. For this purpose, a cryogenic lesion was caused in transgenic animals overproducing IL-10 under the GFAP promoter on astrocytes (GFAP-IL10Tg mice) and the neuro-protection, microglial activation and leukocyte recruitment were evaluated. Our results showed a protective effect of IL-10 on neurons at early time-points after TBI, in correlation with a shift in the microglial activation profile towards a down-regulating phenotype and lower production of pro-inflammatory cytokines. Concomitantly, we observed a reduction in the BBB leakage together with modifications in leukocyte infiltration into the affected area. In conclusion, local IL-10 production modifies the neuro-inflammatory response after TBI, shifting it to anti-inflammatory and neuro-protective conditions. These results point to IL-10 as a promising candidate to improve neuro-inflammation associated with TBI.

Key words: Microglia, Neuro-inflammatory response, Leukocytes, Neuro-degeneration, IL-10R, Cytokines

INTRODUCTION

Traumatic brain injury (TBI) is complex and multifactorial damage, mainly described by primary and secondary injuries. The initial injury is the result of mechanical insult and disruption of brain tissue. Secondary injury processes consist of molecular and biochemical changes that start within minutes after the primary impact, such as inflammation, ischemia, blood brain barrier disruption, vasogenic edema, apoptosis and necrosis. This secondary injury is thus critical in determining the extent of injury expansion and damage to brain tissue following the primary insult [1]. If the incidents that follow brain injury are not controlled in time, they may spread to healthy areas beyond the main area of injury and exacerbate the immune response in the central nervous system (CNS). Thus, urgent care and effective treatment should be available to TBI patients in the short- and long-term to treat their head injuries.

TBI is a heterogeneous disease in terms of cause, pathology, severity and prognosis [2]. Significant consequences of TBI are that more than half of the survivors are moderately or severely disabled one year after injury [3]. Apart from permanent physical disabilities, TBI can be recognized as a chronic process associated with many irreversible pathological conditions. Increased symptoms of seizures, sleep disorders, neuro-degenerative diseases, psychiatric diseases, sexual dysfunction, bladder and bowel incontinence, and systemic metabolic dysregulation may arise and/or persist for

Submitted August 26, 2021, Revised June 18, 2022,
Accepted June 18, 2022

*To whom correspondence should be addressed.
TEL: 34935811826, FAX: 34935812392
e-mail: beatriz.almolda@uab.cat

months to years after injury [4]. Regardless of progression in understanding the pathophysiological processes of TBI over the last few decades, many unanswered questions are still unclear.

Indeed, no effective treatment has been approved for TBI by any health agency in the world. Among the complex cascade of secondary events, neuro-inflammation is a major pathological process in the post-TBI secondary response. Neuro-inflammation is sometimes considered a double-edged sword, as it can induce both detrimental and healing effects [5-8]. A better understanding of the neuro-inflammatory response may help, then, in finding a good therapy for TBI.

Interleukin-10 (IL-10) is an anti-inflammatory and potent inhibitory regulatory molecule that negatively controls CNS glial cells activation and peripheral immune cell responses [9, 10]. IL-10 is produced by different cell types such as T cells (Th2), B cells, macrophages and mast cells. Specifically in the CNS, microglia and astrocytes are the main producers of IL-10 under a wide range of inflammatory situations [11-13]. At the same time, microglia and astrocytes, but also oligodendrocytes, and even neurons, have been reported to express the IL-10 receptor (IL-10R), under both physiological and pathological conditions [13-17]. Furthermore, IL-10 administration suppresses microglial and astroglial activation, as well as decreasing production of pro-inflammatory cytokines [18-20] and leukocyte infiltration [21]. The neuro-protective effect of anti-inflammatory IL-10 treatment has been studied after traumatic spinal cord injury, focal stroke and excitotoxicity [20, 22, 23]. However, contradictory effects have been observed, depending on the type of treatment and especially the route of administration. Thus, intraparenchymal IL-10 administration prevented the development of experimental autoimmune encephalomyelitis (EAE), whereas the systemic administration of this same cytokine has no effect [24] or worsened the disease [25]. Moreover, only systemic IL-10 administration improves the functional outcome after excitotoxicity and traumatic brain injury [23, 26]. These results demonstrate that the route of administration of IL-10 impacts the effects of this cytokine in the evolution of different pathologies of the CNS.

In this context, and to evaluate the effects of IL-10 locally in the CNS, our research group generated a new transgenic animal that overproduces this cytokine under the control of the GFAP promoter on astrocytes [27]. Under homeostatic conditions, this GFAP-IL10Tg mouse line showed modifications in the number and phenotype of microglia in different regions of the brain, such as cortex, hippocampus and cerebellum, including changes in the expression of different microglial markers such as Iba1, CD11b, CD16/32 and F4/80, both in the adult [27] and during aging [28]. Furthermore, neuro-protective effects have been observed in GFAP-IL10Tg animals after different experimental injury models, such as facial nerve axotomy [29] and perforant pathway transection (axonal anterograde degeneration) [30], accompanied by significant changes in the pattern of microglial activation and immune cell infiltration.

Thus, the main objective of this study is to determine the effects that local overexpression of IL-10 produces on neuro-protection and the inflammatory response associated with a traumatic brain injury.

MATERIALS AND METHODS

Animals

Adult transgenic (GFAP-IL10Tg) mice and their corresponding Wild-type (WT) littermates between four-five months old of both sexes were used. GFAP-IL10Tg mice have been designed, created and characterized by our group [27]. All animals were maintained and housed in their home cages at an appropriate temperature (24℃±2℃) with a 12-hour light-dark cycle and *ad libitum* access to water and food.

All experimental animal work was conducted according to Spanish regulations (Ley 32/2007, Real Decreto 1201/2005, Ley 9/2003 and Real Decreto 178/2004) in agreement with European Union directives (86/609/CEE, 91/628/CEE and 92/65/CEE) and was approved by the Ethics Committee of the Autonomous University of Barcelona.

Cryogenic brain injury

Wild-type (WT) and transgenic (GFAP-IL10Tg) mice were anesthetized with an intraperitoneal injection (i.p.) of Ketamine (80 mg/Kg) and Xylazine (20 mg/Kg) at a dose of 0.01 ml/gr per animal. The head of the animals was shaved and skin cut to expose the skull. The cryogenic lesion was caused on the right parietal skull, 2.5 mm posterior and 2.5 mm lateral from Bregma. A metal device having a caoutchouc holder with a tip diameter of 2 mm was kept in liquid nitrogen (-196℃) and placed on the target point for 30 seconds contact time. Wounds were closed by standard skin suture (Laboratory Arago.S.L-6/0) and disinfected by iodine solution [31, 32]. These injured animals were placed in the warmer pad for recovery and returned to their home cage until sacrifice.

Experimental groups

Non-lesioned (NL) and lesioned animals (at 24 hours (hpi), 3 and 7 days post-injury (dpi)) were distributed in different experimental groups and analyzed for immunohistochemistry (IHC), flow cytometry and protein analysis. A total of 89 WT and 93 GFAP-IL10Tg animals were used for IHC, 20 WT and 20 GFAP-

IL10Tg for flow cytometry, 19 WT and 19 GFAP-IL10Tg for protein analysis.

Tissue processing for histological analysis

Animals were deeply anesthetized with the same Ketamine (80 mg/Kg) and Xylazine (20 mg/Kg) solution described above, but at a dose of 0.015 ml/gr per animal and intracardially perfused with 4% paraformaldehyde buffer (4%PFA in Tris-buffer saline 0.1M pH 7.4 (TBS)) for 10 min. The intact brain of each animal was quickly removed and post-fixed in the same fixative solution for 4 h at 4℃, cryo-protected with 30% sucrose solution in 0.1 M phosphate buffer for 48 h at 4℃ and, finally, brains were frozen in cold 2-methyl butane (-55℃ to -60℃) (320404, Sigma-Aldrich; St. Louis) and stored at -20℃. Stored frozen samples were cut into 30 μm parallel coronal sections using a cryostat (CM 3050S Leica), mounted on the SUPERFROST® PLUS slides, dried in the oven at 37℃ for 6 h and stored at -20℃ until used.

Toluidine blue staining

One series of NL and lesioned (24 hpi, 3 dpi, 7 dpi) WT and GFAP-IL10Tg animals were dried for 6 h at RT and incubated in toluidine blue solution (0.1% toluidine blue diluted in acetate Walpole buffer (0.05 M, pH 4.5) for 1 min at RT. After that, slides were washed with distilled water and dehydrated by graded alcohols (50%, 70%, 90%, 100% ethanol), treated with xylene and cover-slipped with histology mounting media.

Fluoro jade-B staining

Sections of TBI-lesioned WT and GFAP-IL10Tg animals at all time-points (24 hpi, 3 dpi, 7 dpi) were dried for 6 h at RT. After incubating in potassium permanganate oxidant solution for 15 min at RT (0.06 gr Mno4K solved in 100 ml dH_2O), sections were rinsed in dH_2O and incubated in 0.01% Fluoro Jade-B (FJ-B) solution for 20 min at RT. For making FJ-B stock solution, 96 ml dH_2O, 1 ml glacial acetic acid and 4 ml Fluoro jade-B solution were mixed. Finally, stained sections were washed with dH_2O, dried and dipped in xylene, and cover-slipped with histology mounting media.

Quantification of degenerating neurons

To study the number of degenerating neurons after TBI in WT and GFAP-IL10Tg animals, sections labeled with FJ-B were analyzed for all time-points. A minimum of nine WT and nine GFAP-IL10Tg animals were used in each time-point. A total of 20 photographs from a minimum of five sections per animal, including the penumbra area of the lesion (PLP) (Fig. 1), were obtained using a 20× lens with a DXM 1200F Nikon digital camera joined to a bright-field Nikon Eclipse 80i microscope, using the ACT-1 2.20 (Nikon Corporation) software. Per each animal, in this analysis, all of the sections in one series were included in which degenerating neurons were observed. Through analySIS® software, the total number of degenerating FJ-B+ neurons was quantified. Data were expressed as FJ-B+ cells/section.

Lesion size quantification

To evaluate the size of the lesion, sections stained with FJ-B were used. A minimum of eight WT and eight GFAP-IL10Tg animals at 24 hpi, 3 dpi and 7 dpi after TBI were analyzed. A minimum of five sections per animal containing the penumbra area was analyzed. Photos of each section were captured using 4× magnification with a DXM 1200F Nikon digital camera joined to a bright-field Nikon Eclipse 80i microscope, using the ACT-1 2.20 (Nikon Corporation) software. Before quantification, all photos of the same section were merged in a single photo by Photoshop® CC software. For each final photo, the affected area, as well as the volume of the total ipsilateral hemisphere and the lateral ventricle of the affected area, were measured using analySIS® software. To determine the corrected affected area, and delete the putative brain swelling or edema, the volume of the lateral ventricle of the affected area was deducted from the ipsilateral hemisphere for each section. The volume of the affected area for each section was then calculated by multiplying section thickness by the number of series and the corrected quantified affected area. The total affected volume of each animal was obtained by averaging all of the section's volume

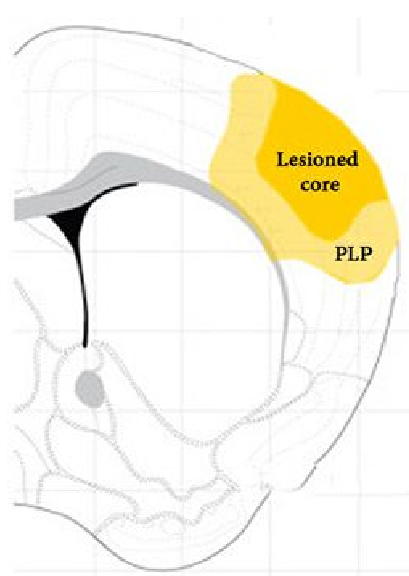

Fig. 1. Scheme illustrating the lesioned core (dark yellow) and the penumbra part (PLP) (light yellow) used to perform all quantifications throughout the study. Adapted from Perego et al. 2011 [33].

of the affected area. The coronal section corresponding to -0.38 mm distance from Bregma (the area where the center of the lesion is located) was considered as a zero point and injured frontal and caudal sections were compared with this Bregma point.

Immunohistochemistry

In this work, the microglial activation, morphology and distribution were analyzed using Iba1 (Ionized calcium binding adaptor molecule), microglial cell density with Pu.1 (myeloid cell transcription factor), microglial proliferation with phosphohistone 3 (pH3), microglia phagocytosis with CD68 (lysosome-associated glycoprotein) and TREM2 (triggering receptor expressed on myeloid cells 2), the neutrophil and lymphocyte recruitment by MPO (myeloperoxidase) and CD3 (cluster of differentiation 3), respectively, and, finally, the BBB permeability by IgG (serum protein) (Table 1).

In all cases, sections were washed with TBS (0.05 M, pH 7.4) and TBS with 0.1% of Triton (TBST) (pH 7.4) and incubated in 70% methanol+2% H_2O_2 for 10 minutes, to block the endogenous peroxidase reactivity. Then, sections were incubated with blocking buffer (BB) containing 90 ml TBST+10 ml FBS+0.3% BSA for 1 h at room temperature (RT). In the case of Pu.1, sections were firstly treated with antigen retrieval solution, containing sodium citrate buffer (pH 8.5, at 80℃ for 40 min). Subsequently, sections were incubated overnight at 4℃ followed by 1 h at RT with primary antibody diluted in the same BB (Table 1). Sections incubated with the same BB lacking the primary antibody were used as a negative control. Following this, sections were rinsed with TBST and incubated with the corresponding biotinylated secondary antibody for 1 h at RT. After washing with TBST, sections were incubated with horseradish peroxidase-conjugated streptavidin diluted in the same BB for 1 h at RT. Finally, after washing with TBS and TB, the immune reaction was visualized by incubating sections with 3,3-diaminobenzidine (DAB) solution (90 ml TB+0.05 g DAB powder+33 μl H_2O_2). Sections were dehydrated in graded alcohol, treated with xylene and cover-slipped with histology mounting media.

Densitometric analysis

To study microglial reactivity, quantitative densitometric analysis of sections stained with Iba1, CD68 and TREM2 was performed. For each immunohistochemistry, a minimum of five TBI-lesioned WT and five TBI-lesioned GFAP-IL10Tg animals in each time-point (24 hpi, 3 and 7 dpi), as well as four NL WT and four NL GFAP-IL10Tg animals were analyzed. Five sections from each animal and time-point, including two areas of interest (the lesioned core and the penumbra part (PLP) (Fig. 1)), were analyzed. Three photos of each section were captured at 20× magnification with a DXM 1200F Nikon digital camera joined to a bright-field Nikon Eclipse 80i microscope, using the ACT-1 2.20 (Nikon Corporation) software. For each photograph, both the percentage of area occupied by the immunostaining (%Area) and the intensity of the immunoreaction (Mean Gray Value) were calculated using the analySIS® software. The level of immunoreactivity (AI) was calculated by multiplying the percentage of the area and the intensity of immunolabeling.

Table 1. List of antibodies and reagents used for immunohistochemistry

	Target antigen	Host	Dilution	Cat number	Manufacturer
Primary antibody	Iba1	Rabbit	1:1,000	019-19741	Wako
	Pu.1	Rabbit	1:400	2258S	Cell Signalling
	pH3	Rabbit	1:3,000	06-570	Millipore
	MPO	Rabbit	1:100	9535	Abcam
	CD68	Rat	1:1,000	MAC 1957	BIO-RAD
	TREM2	Sheep	1:200	F1729	R&D Systems
	GFAP	Mouse	1:100	G3893	Sigma-Aldrich
	IL-10R	Rabbit	1:50	Sc-985	Santa Cruz
	CD11b	Rat	1:100	MCA711G	AbD Serotec
	CD3	Hamster	1:250	MCA2690	AbD Serotec
Secondary antibody	Biotinylated	Rabbit	1:500	BA-1000	Vector Laboratories
	Biotinylated	Rat	1:500	BA-4001	Vector Laboratories
	Biotinylated	Sheep	1:500	BA-6000	Vector Laboratories
	Biotinylated	Hamster	1:500	BA-9100	Vector Laboratories
	Biotinylated	Mouse	1:500	BA-2001	Vector Laboratories
	Alexa 488	Mouse	1:500	A11029	Invitrogen
	Alexa555	Rabbit	1:500	A21428	Invitrogen
Streptavidin –HRP			1:500	SA-5004	Vector Laboratories
Streptavidin-Alexa Fluor 555			1:500	S21381	Life Technologies
Streptavidin-Alexa Fluor 488			1:500	S11223	Invitrogen
DAPI			1:10,000	9542	Sigma -Aldrich

 https://doi.org/10.5607/en21035

For the quantification of the microglial cell density, sections stained with Pu.1 were used. A minimum of three TBI-lesioned WT and three TBI-lesioned GFAP-IL10Tg animals at all time-points, and four NL WT and four NL GFAP-IL10Tg mice were used. A minimum of five sections from each animal, including both the lesioned core and the PLP part, were analyzed. Three photos of each section were captured with 20× magnification using the same device and software specified above. The number of Pu.1+ nuclei was obtained by the "Automatic Cell Counter" (ITCN) plug-in from NIH Image J software (Wayne Rasband, National Institutes of Health, USA). Data were expressed as cells/mm^2.

Quantification of microglial cell proliferation was performed on sections immunolabeled for the mitotic marker phosphohistone 3 (pH3) in both NL and TBI-lesioned animals at 24 hpi, 3 dpi and 7 dpi. At least three WT and three GFAP-IL10Tg animals were analyzed. The number of pH3 positive cells was manually counted on five different sections per animal using a 20× lens. Data were averaged and expressed as pH3+ cells/section.

To evaluate neutrophil migration after TBI, sections stained with MPO were used. A minimum of three WT and three GFAP-IL10Tg animals were used for each time-point. At least five different sections of each animal were studied. A minimum of three photos of each section were captured by 40× magnification with a DXM 1200F Nikon digital camera joined to a bright-field Nikon Eclipse 80i microscope, using the ACT-1 2.20 (Nikon corporation) software. The number of MPO+ cells of each photo was counted using the Image J software and data were averaged and represented as MPO+/section.

Quantification of lymphocyte infiltration was carried out on sections immunolabeled with CD3 at 3 dpi and 7 dpi after TBI. At least five WT and five GFAP-IL10Tg animals were analyzed. A minimum of five different sections of each animal was captured at 20× magnification using the same device and software specified above. Data were averaged and expressed as CD3+/section.

To evaluate BBB disruption after TBI, a minimum of three WT and three GFAP-IL10Tg animals were used at 24 hpi and 3 dpi. At least five sections of each animal immunolabeled with IgG were studied. Each section was photographed using the 2× magnification and the area occupied by the IgG staining was measured. Data were averaged and expressed as μm^3.

Double immunofluorescence and confocal analysis

To detect proliferative microglial cells, immunofluorescence combining pH3 and CD11b antibodies was performed. Sections were processed following the same procedure specified in the previous paragraph for pH3 staining, but rather using anti-rabbit Alexa-Fluor® 555 conjugated antibody as a secondary antibody. Then, sections were washed with TBST and incubated for 1 h at RT in BB followed by anti-rat CD11b diluted in BB overnight at 4℃ followed by 1 h at RT. Afterward, sections were washed with TBST and incubated with biotinylated anti-rat secondary antibody for 1 h at RT and then with Alexa-Fluor® 488 conjugated streptavidin diluted in BB for 1 h at RT. Finally, sections were washed with TBST, TBS and TB.

To determine the putative IL-10R co-localization with astrocytes, double immunofluorescence using IL-10R and GFAP was performed. First, sections were dried for 6 h at RT, washed with TBS and TBST and incubated for 1 h at RT with blocking buffer solution 2 (BB2), containing 0.2% gelatin (powder food grade, 104078, Merck; Burlington, Massachusetts, USA) in TBST. After this, sections were incubated with anti-rabbit IL-10R antibody for 48 h at 4℃ followed by 1 h at RT (Table 1). After washing with TBST, sections were incubated with biotinylated anti-rabbit antibody diluted in BB2 for 1 h at RT, followed by incubation with Alexa-Fluor® 555 conjugated with streptavidin diluted in BB2 for 1 h at RT. Sections were next washed with TBST and incubated with BB containing 90 ml TBST+10 ml FBS+0.3 g BSA for 1 h at RT. The experiment was followed by incubation with anti-mouse GFAP diluted in BB overnight at 4℃ followed by 1 h at RT, and with anti-mouse Alexa Fluor® 488 diluted in BB for 1 h at RT (Table 1).

All double-labeled sections were counterstained with 4,9,6-diamidino-2-phenylindole (DAPI) diluted in TB for 10 min, before being cover-slipped with Fluoromount G™ (0100-01; SouthernBiotech; Birmingham, AL). Negative controls were performed by incubating the sections with the corresponding BB, but without the primary antibodies.

Flow cytometry analysis

The phenotype of microglia and monocyte/macrophage populations, in NL and TBI-lesioned animals (at 24 hpi and 3 dpi) was analyzed using flow cytometry, as previously described [34]. Briefly, anesthetized animals were intracardially perfused for 1 min with 0.1 M phosphate buffer solution (PBS), the brain was removed and the cortex was quickly dissected out. To obtain a cell suspension, samples were dissociated through 140 μm and 70 μm meshes and digested for 30 min at 37℃ using type IV collagenase (17104-019, Life Technologies) and DNAase I (D5025, Sigma). Subsequently, each cellular suspension was centrifuged at RT for 20 min at 2,400 rpm in a discontinuous, density Percoll gradient (17-0891-02, Amersham-Pharmacia) between 1.03 g/ml and 1.08 g/ml. Cells in the interphase and the clear upper-phase were collected, washed in PBS+2% serum, and the Fc receptors were blocked by incubation for 10 min at 4℃ in a solution of purified CD16/32 diluted in PBS+2% serum. Afterward, cells were labeled

Table 2. List of antibodies used in flow cytometry

Target antigen	Host	Format	Dilution	Cat number	Manufacturer
Fc blocker	CD16/32	Purified	1:250	553142	BD pharmingen
Primary antibody	CD11b	PE-Cy7	1:400	557657	BD pharmingen
	CD45	PerCP	1:400	557235	BD pharmingen
	CCR2	PE	1:400	150609	Biolegend
	Ly6C	FITC	1:400	553104	BD Biosciences

for 30 min at 4℃ with the following combination of surface antibodies: anti-CD11b-PE-Cy7, anti-CD45-PerCP, anti-CCR2-PE and anti-Ly6C-FITC (Table 2). In parallel, isotype-matched control antibodies for the different fluorochromes were used as negative control, and cell suspension of splenocytes as a positive control. Data were extrapolated as the number of cells using Cyto CountTM fluorescent beads, following the manufacturer's instructions (S2366, Dako Cytomation). Finally, cells were acquired using a FACS Canto flow cytometer (Becton Dickinson; San Jose, CA) and results were analyzed using the FlowJo® software. The analysis was performed separately for each animal without any pooling.

Tissue processing for protein analysis

Animals used for protein analysis were anesthetized with an intraperitoneal injection (i.p.) of Ketamine (80 mg/Kg) and Xylazine (20 mg/Kg) at a dose of 0.015 ml/gr per animal and intracardially perfused with chilled phosphate buffered saline PBS (0.1M, pH 7.4) for 1 min. The ipsilateral cortex was quickly dissected and snap-frozen individually in liquid nitrogen and stored at -80℃. Total protein was extracted by solubilization of samples on lysis buffer containing 25 mM HEPES, 2% Igepal, 5 mM $MgCl_2$, 1.3 mM EDTA, 1 mM EGTA, 0.1M PMSF, protease (1:100, P8340, Sigma Aldrich) and phosphatase inhibitor cocktails (1:100, P0044, Sigma Aldrich) for 2 h at 4℃. After solubilization, samples were centrifuged at 13,000 rpm for 5 min at 4℃ and the supernatants were collected. Total protein concentration was determined with a commercial Pierce BCA Protein Assay kit (#23225, Thermo Scientific) according to the manufacturer's protocol. Protein lysates were aliquotted and stored at -80℃ until used for protein microarray analysis and ELISA assay.

Cytokines-chemokines analysis

Cytokines IL-1β, TNF-α, IL-10 and chemokines CXCL1 (KC/GRO) and CCL2 (MCP-1) were analyzed using a Milliplex® MAP Mouse Cytokine/Chemokine kit (#MCYTOMAG-70K, Merck Millipore) according to the manufacturer's instructions. Briefly, 25 µl of each cortex extract, with a final total protein concentration of 3 µg/µl were added to the plates, along with the standards in separate wells, containing 25 µl of custom fluorescent beads and 25 µl of matrix solution, and incubated overnight at 4℃ in a plate-shaker (750 rpm). After two washes with wash buffer (1x), the plate was incubated with 25 µl of detection antibodies for 30 min at RT followed by incubation with 25 µl of Streptavidin-Phycoerythrin for 30 min at RT in a plate-shaker (750 rpm). Finally, the plate was washed twice with wash buffer and 150 µl of Drive fluid was added. A Luminex® MAGPIX® device with the xPONENT® 4.2 software was used to read the plate. Data were analyzed using the Milliplex® Analyst 5.1 software and expressed as pg/ml of protein.

TGF-β1 was determined by ELISA assay by using the Human/Mouse TGF-β1 Uncoated ELISA kit (#88-8350, Invitrogen-Thermo Fisher) according to the manufacturer's instructions. Briefly, TGF-β1 target-specific antibody was coated to the ELISA microplate overnight at 4℃ on the shaker. One-hundred µl of each cortex extract with a final total protein concentration of 2.5 µg/µl was added into the wells and incubated overnight at 4℃ in a plate-shaker (750 rpm). After three washes with wash buffer, the plate was incubated with 100 µl of detection antibody for 1 h at RT, followed by 100 µl of avidin-HRP enzyme for 15 min at RT. Lastly, the plate was washed five times in wash buffer and incubated with TMD substrate solution for 15 min. The plate was read in a Bio-Rad iMark microplate absorbance reader at 450 nm and data were expressed as pg/mL of protein.

Statistical analysis

All experimental values were expressed as mean±standard error of the mean (SEM). Graph PadPrism® 6.01 software was used for statistical analysis. The Two-way ANOVA test, with Fisher's Test as a *post-hoc* test to compare among the groups, was used.

RESULTS

General cyto-architecture of brain

To detect possible alterations in the cyto-architecture induced by transgene-encoded IL-10 production in the brain, a microscopic study of toluidine blue stained sections was performed in both NL conditions and after TBI (Fig. 2). Our qualitative analysis demonstrated no differences between NL WT and NL GFAP-IL10Tg mice in the disposition of neuronal layers in the cerebral cortex.

 https://doi.org/10.5607/en21035

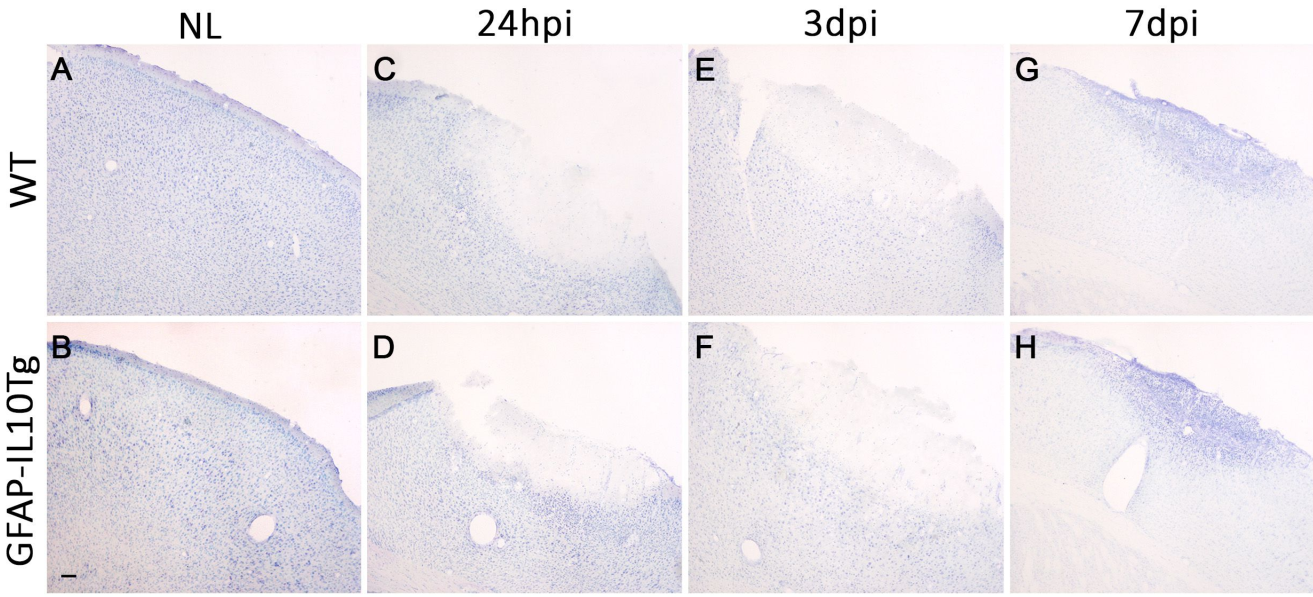

Fig. 2. Toluidine blue staining. Representative images showing the toluidine blue staining of cortex in non-lesioned (NL) WT (A) and NL GFAP-IL10Tg (B) animals. After TBI, both WT (C, E, G) and GFAP-IL10Tg animals (D, F, H) showed the area of lesion in the cortex characterized by a depleted area of neurons surrounded by the penumbra, exhibiting pigmented nuclei indicative of degeneration from 24 hpi to 7 dpi. No differences between WT and GFAP-IL10Tg animals were detected at any time-point studied. Scale bar=100 μm.

After TBI, at 24 hpi, a depleted area of cells was observed in the lesioned core of WT animals surrounded by an area of cells with pyknotic nuclei, corresponding to the penumbra area (PLP). The number of pyknotic cells in the PLP progressively decreased from 3 dpi to 7 dpi, whereas in the lesioned core it was not until 7 dpi that an area densely occupied by cells was detected. No apparent differences between WT and GFAP-IL10Tg mice were found at any time-point analyzed in either the lesioned core or the PLP area (Fig. 2).

Neuronal degeneration and lesion volume

In order to study the effect of IL-10 on neuronal degeneration, sections were stained with Fluoro Jade-B (FJ-B), a marker associated with degenerating neurons (Fig. 3). FJ-B+ neurons were observed in the PLP area, just surrounding the lesioned core, in both WT and GFAP-IL10Tg mice, with a maximum number at 24 hpi and progressively decreasing afterward (Fig. 3A~F). A significant decrease in the number of FJ-B+ cells was reported in GFAP-IL10Tg at early time-points (24 hpi and 3 dpi), when compared with WT (Fig. 3G).

FJ-B immunostained sections were also used to measure lesion size. No detectable differences in the lesion volume or the spread of the lesion were observed between WT and GFAP-IL10Tg animals at any time-point studied (Fig. 3H~J).

Analysis of microglial/macrophage cell morphology, distribution and density

CD11b+/CD45+ Cells/Cell populations

By flow cytometry, we assessed possible modifications in the number of microglia/macrophage populations induced by the transgenic production of IL-10 in the ipsilateral cortex. We also identified the microglia/macrophage population based on the positive CD11b expression in combination with differential expression levels of CD45 (Fig. 4). This helped in differentiating homeostatic from activated microglia as well as macrophages. Thus, ramified or homeostatic microglia was identified as CD11b+/CD-45^{low} and activated microglia as CD11b+/$CD45^{int}$. Moreover, the CD11b+/$CD45^{high}$ population was identified, which may include highly activated microglia, monocytes and macrophages cells. In this study, we have used the term CD11b+/$CD45^{low/int}$ to refer to the population of homeostatic and activated microglia, jointly.

Our results showed no detectable differences in the number of CD11b+/$CD45^{low/int}$ or CD11b+/$CD45^{high}$ cell populations among NL WT and NL GFAP-IL10Tg mice (Fig. 4C, D). However, expression levels of CD45 (mean fluorescence intensity), in GFAP-IL10Tg mice, as compared to WT were higher in the CD11b+/$CD45^{low/int}$ and lower in the CD11b+/$CD45^{high}$ cell population (Fig. 4E, F).

After TBI, WT experimented a significant increase in the number of the CD11b+/$CD45^{low/int}$ cell population at 24 hpi, whereas in

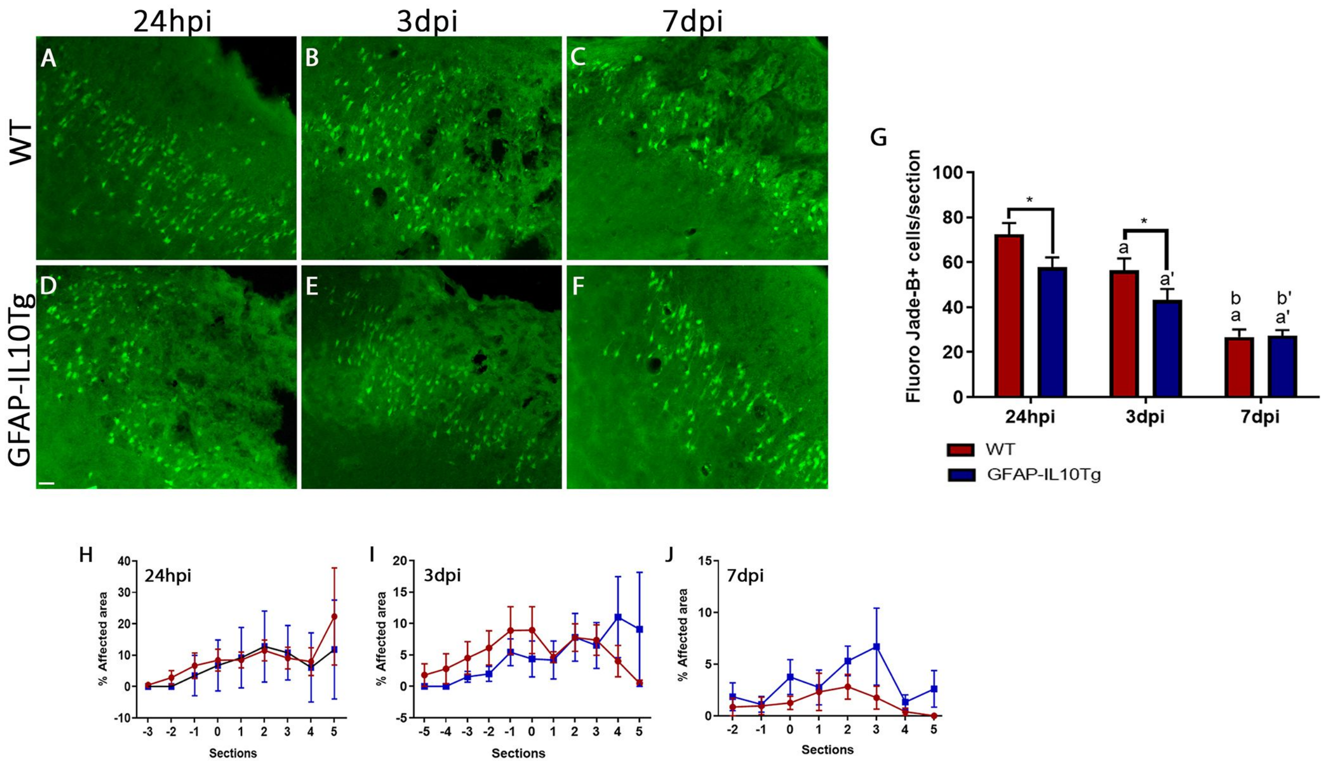

Fig. 3. Fluoro Jade-B staining. (A~F) Representative images revealing Fluoro Jade-B+ neurons (green) indicative of neuronal degeneration within the penumbra area in WT (A~C) and GFAP-IL10Tg animals (D~F). (G) Graph showing the quantification of Fluoro Jade-B (FJ-B)+ cells along the different time-points after TBI. Note that transgenic animals showed lower degenerating neurons, in comparison to WT, at 24 hpi and 3 dpi. (H~J) Graphs showing the quantification of lesion volume at 24 hpi (H), 3 dpi (I) and 7 dpi (J) in both WT and GFAP-IL10Tg animals. No significant differences between WT and GFAP-IL10Tg animals were observed at any time-point analyzed. Data are represented as mean±SEM (*$p \leq 0.05$). In WT animals: "a" indicates significance vs 24 hpi, "b" indicates significance vs 3 dpi. In GFAP-IL10Tg animals: "a'" indicates significance vs 24 hpi, "b'" indicates significance vs 3 dpi. Scale bar=50 μm.

GFAP-IL10Tg mice this increase was observed at 3 dpi (Fig. 4C). In contrast, the CD11b+/CD45^{high} cells were found to similarly increase in both experimental groups at 24 hpi, although at 3 dpi the number was significantly higher in GFAP-IL10Tg animals (Fig. 4D). Moreover, CD45 expression levels were higher in the CD11b+/CD45$^{low/int}$ cell population of GFAP-IL10Tg mice than in WT at all time-points after lesion, whereas it was similar between genotypes in the CD11b+/CD45^{high} populations (Fig. 4E, F).

To assess the specific location, morphology and distribution of microglia/macrophages along the different time-points after TBI, Iba1 immunohistochemistry was performed. Moreover, to analyze putative modifications in the cell density of cells, myeloid marker Pu.1 was used [35]. Our analysis demonstrated a significant increase in Iba1 labeling (Fig. 5A, B, W, Z) as well as in the number of Pu.1+ cells (Fig. 6A, B, I, L) in GFAP-IL10Tg animals in NL conditions, as compared to WT. This increase was associated with morphological changes, such that microglial cells in the cortex of transgenic animals showed an enlargement of the cell body and thicker processes (Fig. 5I, J).

After TBI, both WT and GFAP-IL10Tg animals experienced a remarkable increase in both the Iba1 immunoreactivity and the number of Pu.1+ cells, but with some dissimilarity in the dynamics, depending on the area analyzed.

In the lesioned core of WT, a progressive increase of both Iba1 labeling and Pu.1+ cells were observed in the lesioned core from 3 dpi, whereas in GFAP-IL10Tg animals an initial abrupt decrease of Iba1 expression was detected at 24 hpi that increased afterward at 3 dpi (Fig. 5W, 6I). Remarkably the initial decrease of Iba1 observed in transgenic animals was not detected when Pu.1 was quantified.

In the PLP part, WT animals showed an up-regulation in the Iba1 labeling and in the number of Pu.1+ cells at 3 dpi that remained stable at 7 dpi. Similar to the lesioned core, the initial decrease of cells at 24 hpi was only found in GFAP-IL10Tg mice.

Principal differences between WT and GFAP-IL10Tg mice were found in the lesioned core, showing a higher number of Pu.1+ cells

https://doi.org/10.5607/en21035

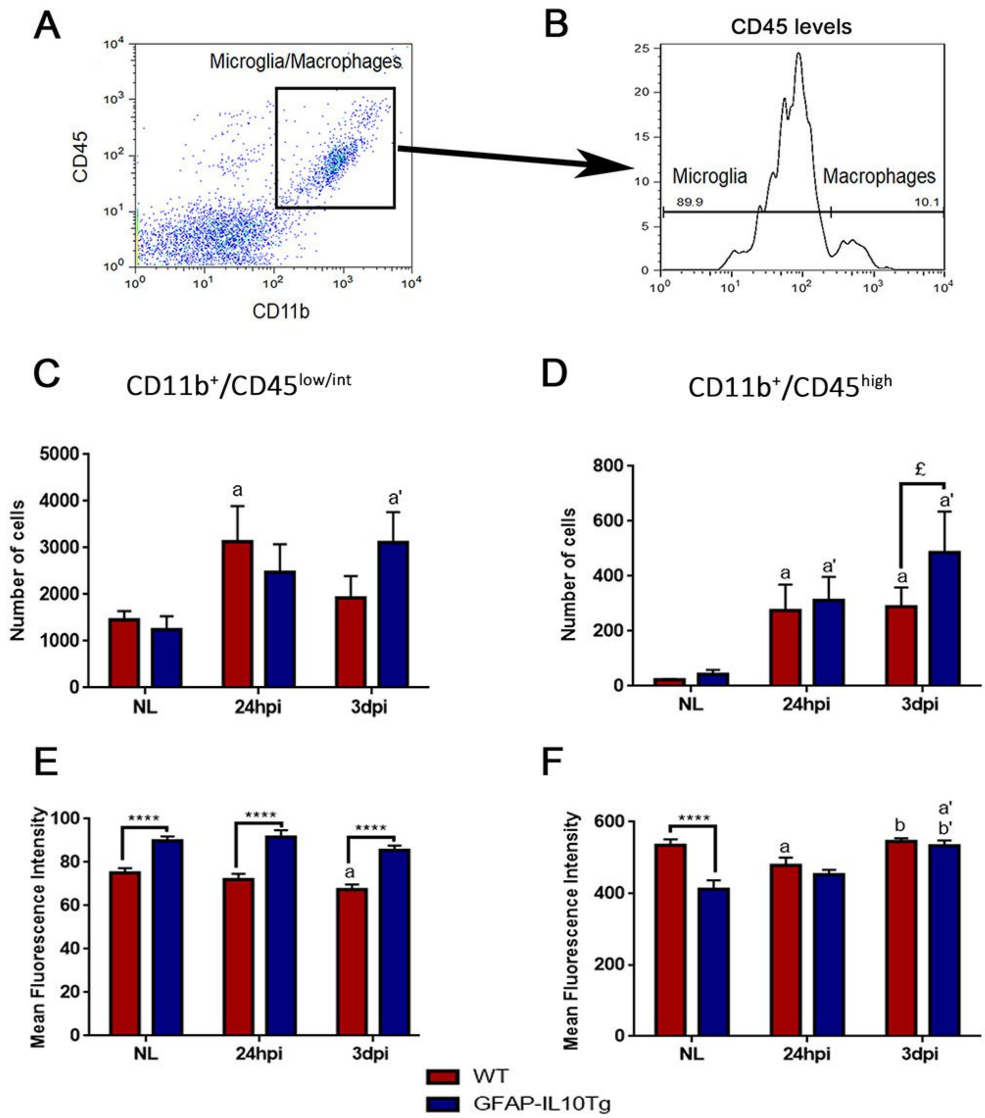

Fig. 4. Microglia and Macrophage populations. (A) Representative density plot of CD11b+/CD45+ cells in the cortex. (B) Histogram showing the gating strategy to study microglia (CD11b+/CD45$^{low/int}$) and macrophage (CD11b+/CD45^{high}) cells. (C, D) Graphs showing the number of cells in the microglia (CD11b+/CD45$^{low/int}$) and the macrophage (CD11b+/CD45^{high}) populations in the cortex of non-lesioned (NL) and TBI-lesioned animals at 24 hpi and 3 dpi in WT and GFAP-IL10Tg animals. (E, F) Graphs showing the intensity of CD45 in microglia (CD11b+/CD45$^{low/int}$) and macrophage (CD11b+/CD45^{high}) populations of non-lesioned (NL) and lesioned animals at 24 hpi and 3 dpi, in both WT and GFAP-IL10Tg mice. All values are indicated as mean±SEM ($^{£}$p≤0.1, ****p≤0.0001). In WT animals: "a" indicates significant vs NL, "b" indicates significant vs 24 hpi. In GFAP-IL10Tg animals: "a'" indicates significant vs NL, "b'" indicates significant vs 24 hpi.

at early time-points (3 dpi) (Fig. 6I) and lower Iba1 expression later on (7 dpi) in transgenic animals (Fig. 5W).

To graphically represent the dynamics of microglial activation following TBI in both WT and GFAP-IL10Tg animals, the fold changes, with respect to their corresponding NL animals, were calculated. This representation revealed that the up-regulation of Iba1 and Pu.1, with respect to its basal levels, was less pronounced in GFAP-IL10Tg animals than in WT at all time-points analyzed (Fig. 5X, Y, A', B', 6J, K, M, N).

Moreover, after TBI, remarkable changes in the morphology of activated microglia in the lesioned core and PLP were also observed, depending on the time post-injury in both genotypes. The characteristic, ramified cells with low ramifications became foamy-amoebic forms at 3 dpi, especially in the lesioned core (Fig. 5O, P) and finally appeared as cells with elongated cell nuclei and thick and short processes at 7 dpi (Fig. 5S~V). No detectable differences between WT and GFAP-IL10Tg animals were observed in terms of microglial morphology at any time-point studied.

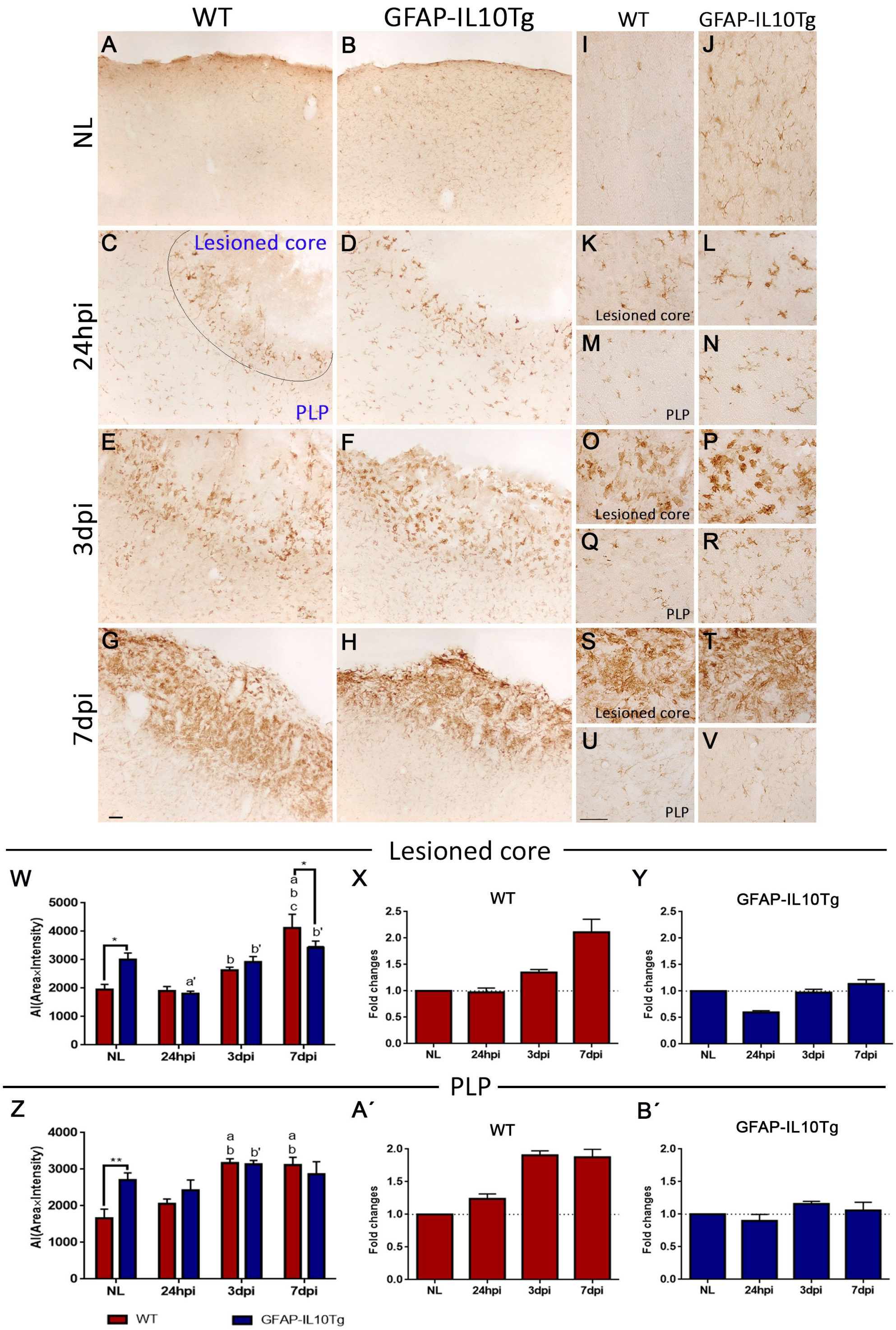

Fig. 5. Iba1 immunohistochemistry. (A~V) Representative images from WT and GFAP-IL10Tg animals showing Iba1 immunoreactivity in the cortex of non-lesioned (NL) (A, B, I, J), and in the affected area of TBI-injured animals from 24 hpi to 7 dpi (C~H, K~V). (W, Z) Graphs showing the quantification of Iba1 immunoreactivity as the AI (Area ^{x} Intensity) after TBI at lesioned core (W) and PLP (Z). Note that microglia in NL GFAP-IL10Tg animals (W, Z) showed higher Iba1 immunoreactivity than did WT, associated with thicker and elongated morphologies (I, J). After TBI, a reduction of Iba1 labeling was observed in transgenic animals at 7 dpi in the lesioned core (W). (X, Y, A', B') Graphs showing the fold changes of Iba1 expression, in comparison to the respective NL animals in WT (X, A') and GFAP-IL10Tg (Y, B') animals in the affected area. GFAP-IL10Tg animals showed a significant lower fold increase of Iba1 than did WT in both lesioned core and PLP parts. All values corresponded to mean±SEM (*p≤0.05, **p≤0.01). In WT animals: "a" indicates significant vs NL, "b" indicates significant vs 24 hpi, "c" indicates significant vs 3 dpi. In GFAP-IL10Tg animals: "a'" indicates significant vs NL, "b'" indicates significant vs 24 hpi. Scale bar=50 µm.

https://doi.org/10.5607/en21035

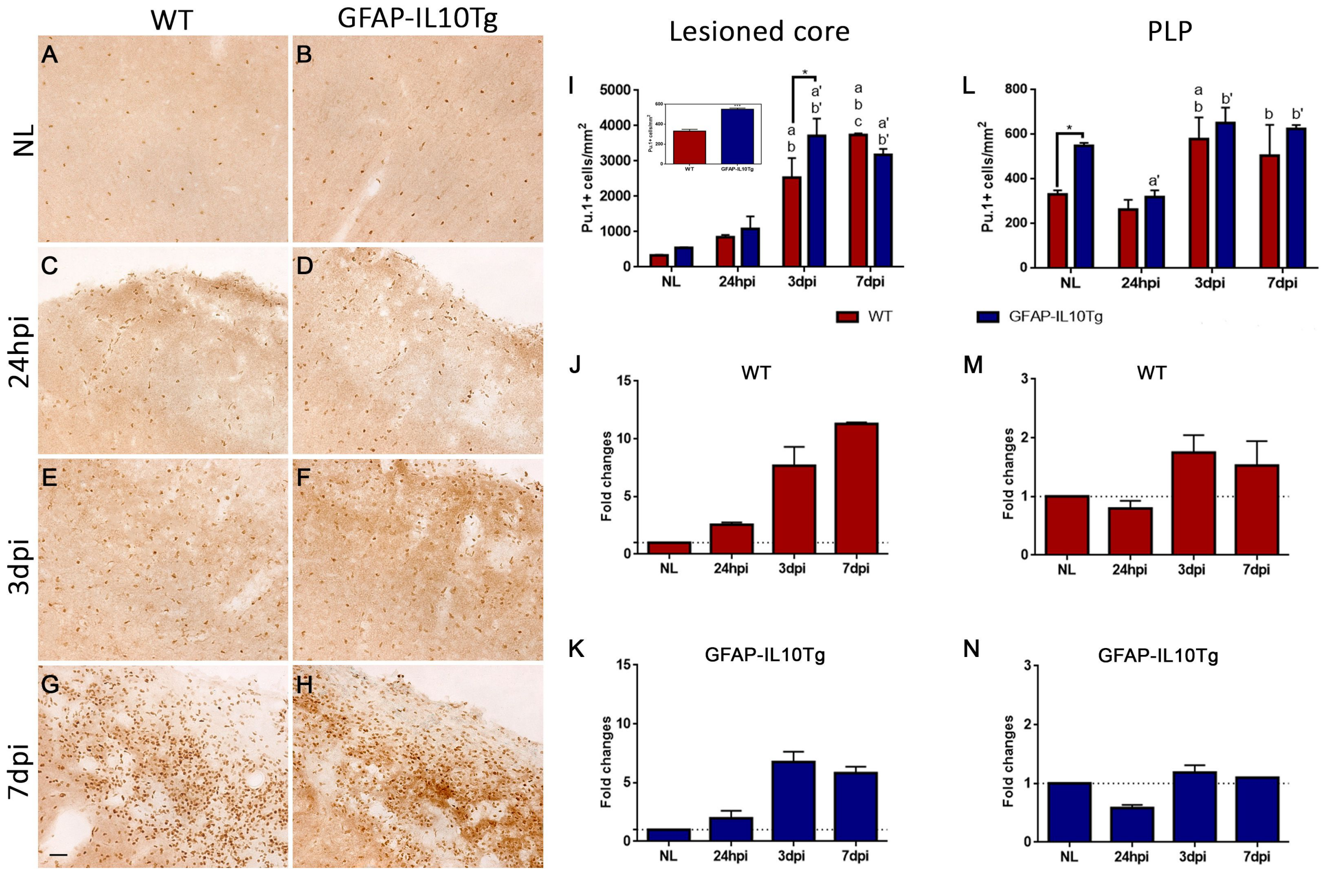

Fig. 6. Pu.1 immunohistochemistry. (A~H) Representative images showing Pu.1+cells in the NL WT (A) and NL GFAP-IL10Tg (B) as well as the lesioned core of both WT (C, E, G) and GFAP-IL10Tg (D, F, H) animals. (I, L) Graphs showing the quantification of Pu.1+ cells of both WT and GFAP-IL10Tg in non-lesioned (NL) and lesioned animals from 24 hpi to 7 dpi in the lesioned core (I) and PLP part (L). Note that GFAP-IL10Tg animals showed a higher number of Pu.1+cells in NL (insert in I) and at 3 dpi. (J, K, M, N) Graphs showing the fold change of Pu.1+ cells in WT (J, M) and GFAP-IL10Tg (K, N), in comparison to their corresponding NL animals. Note that, in GFAP-IL10Tg mice, the fold increase of Pu.1+ cells along the injury is less pronounced than in WT, especially at 7 dpi in the lesioned core. All values are indicated as mean±SEM (*p≤0.05, ***p≤0.001). In WT animals: "a" indicates significance vs NL, "b" indicates significance vs 24 hpi, "c" indicates significance vs 3 dpi. In GFAP-IL10Tg animals: "a'" indicates significance vs NL, "b'" indicates significance vs 24 hpi. Scale bar=30 μm.

Microglial proliferation

In order to study whether changes observed in microglial cell density were related to modifications in proliferation, sections were labeled for the cell proliferation marker phosphohistone 3 (pH3). Few pH3+ cells were found in NL WT and NL GFAP-IL10Tg animals without differences between genotypes. After TBI, both groups of animals underwent a drastic increase in the number of pH3+ cells at 24 hpi (Fig. 7A, B). In WT animals, this increase continued until 3 dpi (Fig. 7C) and decreased thereafter at 7 dpi (Fig. 7E). In contrast, in GFAP-IL10Tg mice, the number of pH3+ cells decreased significantly at 3 dpi and remained constant at later time-points (Fig. 7D, F). The comparison between genotypes showed that the number of pH3+ cells at 3 dpi was significantly higher in WT animals than in GFAP-IL10Tg (Fig. 7G).

To analyze the phenotype of proliferating cells, a double immunofluorescence combining CD11b (pan-microglia/macrophages marker) and pH3 was performed. Quantification of double CD11b+/pH3+ cells indicated that almost all pH3+ cells corresponded to microglia/macrophages in both WT and GFAP-IL10Tg animals (Fig. 7I, J) and confirmed the lower amount of double-positive cells in transgenic animals at 3 dpi, when compared to WT (Fig. 7H).

Microglial phagocytic phenotype

In order to investigate the putative changes that transgenic IL-10 production may exert on the phenotype of the microglia/macrophage cells along the different time-points after TBI, the expression of two markers related to the phagocytic function of this cell population, CD68 and TREM2, was analyzed.

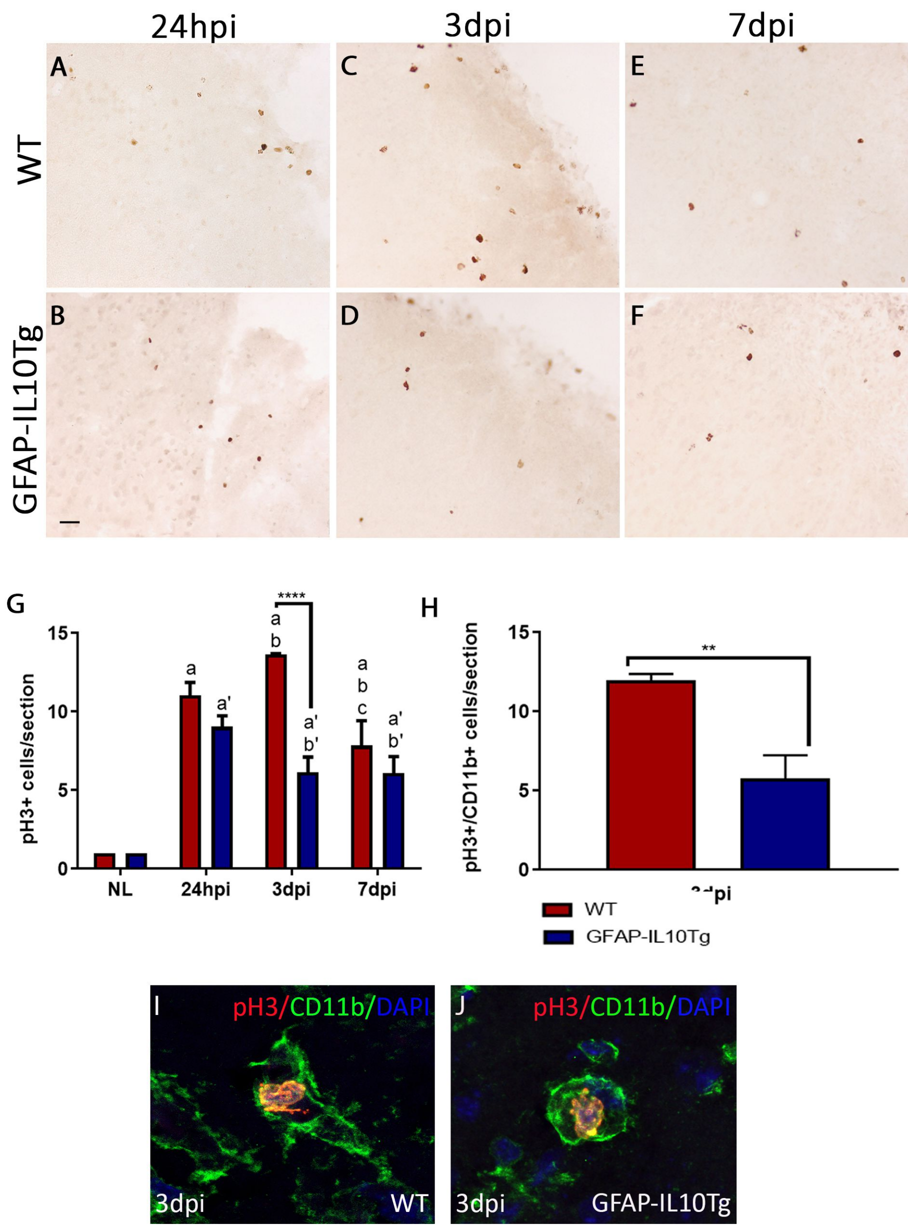

Fig. 7. Microglial/Macrophage proliferation. (A~F) Representative images showing the number of proliferating pH3+ cells in the penumbra of lesioned animals of both WT (A, C, E) and GFAP-IL10Tg animals (B, D, F). (G) Graph showing the quantification of pH3+ cells/section in non-lesioned (NL) and lesioned animals from 24 hpi to 7 dpi in both WT and GFAP-IL10Tg animals. (H) Graph showing the quantification of microglia/macrophage (pH3+/CD11b+) cells/section at 3 dpi in both WT and GFAP-IL10Tg animals. Note that, in GFAP-IL10Tg animals, the number of proliferating microglia/macrophages was significantly low, as compared with WT (**p≤0.01, ****p≤0.0001). (I, J) Representative images of double immunofluorescence of pH3 (red) and CD11b (green) at 3 dpi from WT (I) and GFAP-IL10Tg (J) animals. Nuclei of cells were counterstained with DAPI (blue). All data are represented as mean±SEM. In WT animals: "a" indicates significant vs NL, "b" indicates significant vs 24 hpi, "c" indicates significant vs 3 dpi. In GFAP-IL10Tg animals: "a'" indicates significant vs NL, "b'" indicates significant vs 24 hpi. Scale bar=30 μm.

CD68 staining

Very low expression of CD68 was detected in NL animals of both genotypes without remarkable differences between them. After TBI, a significant increase in the CD68 expression levels was observed, in both WT and GFAP-IL10Tg animals, at 3 dpi and 7 dpi in the two areas analyzed (Fig. 8A~C, F~H). However, levels were higher in GFAP-IL10Tg animals at 3 dpi in both areas (Fig. 8C, H). At this time-point, CD68+ microglia showed a bushy morphology in both WT and GFAP-IL10Tg animals, especially in the lesioned core, without differences in any of the groups (Fig. 8A, B).

 https://doi.org/10.5607/en21035

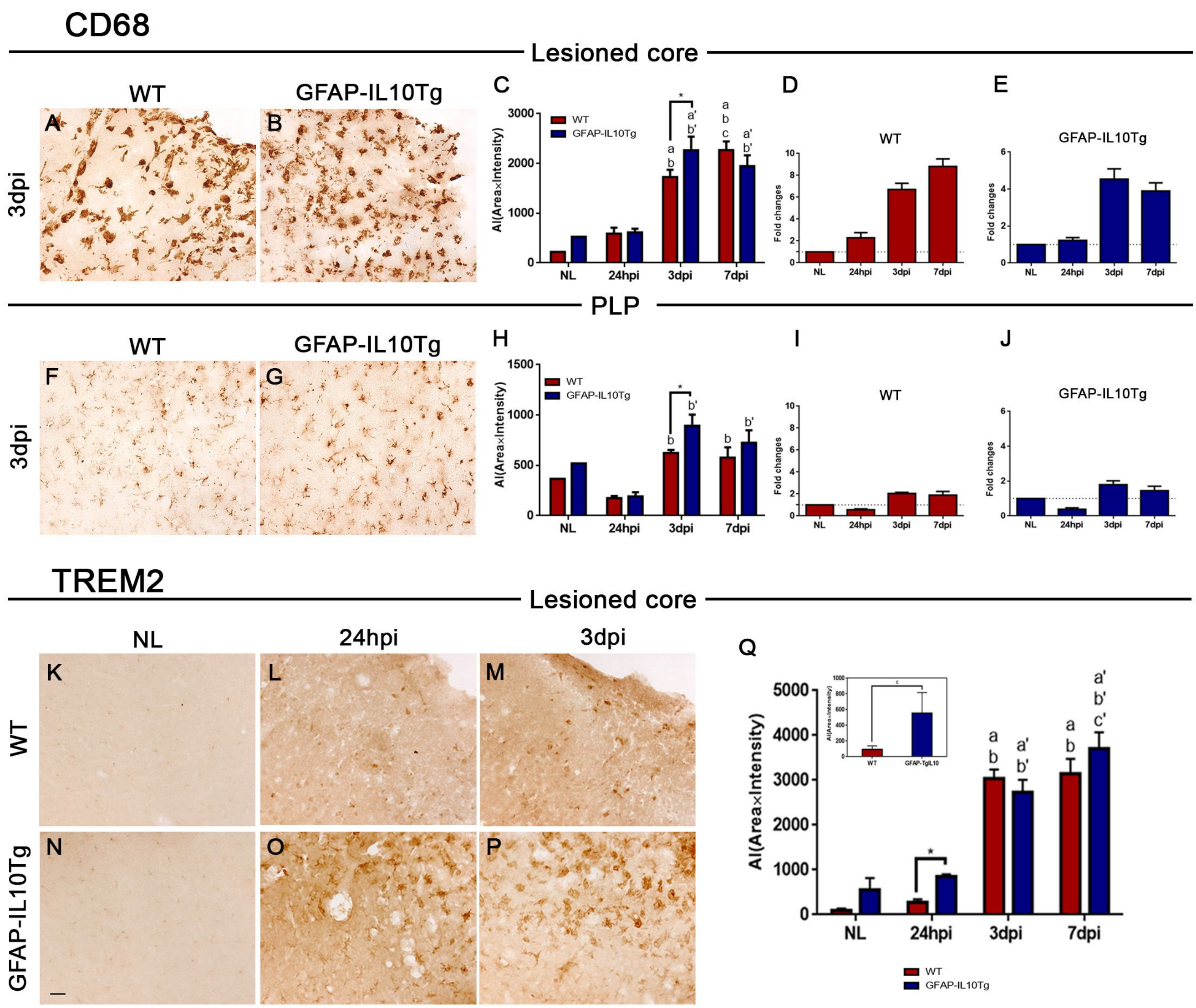

Fig. 8. Phagocytotic microglia. (A, B, F, G) Representative images of CD68 immunolabeling in the lesioned core (A, B) and PLP area (F, G) of WT (A, F) and GFAP-IL10Tg animals (B, G) at 3 dpi. (C, H) Graphs showing the quantification of CD68 immunoreactivity as the AI (Area x Intensity) of both WT and GFAP-IL10Tg in non-lesioned (NL), lesioned core (C) and PLP part (H) in lesioned animals from 24 hpi to 7 dpi. Note that GFAP-IL10Tg animals showed higher expression of CD68 at 3 dpi in both areas. (D, E, I, J) Graphs showing the fold changes of CD68 expression in comparison to the respective NL animals in WT (D, I) and GFAP-IL10Tg animals (E, J) in the lesioned core and PLP. GFAP-IL10Tg animals showed a significant, lower fold increase of CD68 than did WT in both lesioned core and PLP. (K~P) Representative images of TREM2 immunoreactivity in both the non-lesioned (NL) (K, N) and lesioned core of TBI-injured mice at 24 hpi (L, O) and 3 dpi (M, P) in WT (L, M) and GFAP-IL10Tg groups (O, P). (Q) Graph showing the quantification of TREM2 immunoreactivity as the AI (Area x Intensity) in non-lesioned (NL) and at the lesioned core of lesioned animals from 24 hpi to 7 dpi. Note that GFAP-IL10Tg animals showed higher expression of TREM2 in NL animals (inset in Q) and at 24 hpi in the lesioned area. All values are represented as mean±SEM (εp≤0.1, *p≤0.05). In WT animals: "a" indicates significant vs NL, "b" indicates significant vs 24 hpi, "c" indicates significant vs 3 dpi. In GFAP-IL10Tg animals: "a'" indicates significant vs NL, "b'" indicates significant vs 24 hpi, "c'" indicates significant vs 3 dpi.

Moreover, the analysis of fold changes for this marker, similar to the results obtained for Iba1 and Pu.1, demonstrating that, despite the increase in CD68 labeling in transgenic animals, the up-regulation of this marker in comparison to their NL conditions was less pronounced in GFAP-IL10Tg than in WT in both lesioned core and PLP (Fig. 8D, E, I, J).

TREM2 staining

In NL conditions, an increase in TREM2 expression was observed in GFAP-IL10Tg mice (Fig. 8K, N). After TBI, TREM2 levels showed an abrupt increase at 3 dpi in both WT and transgenic animals which was more pronounced in the lesioned core than in the PLP. In the lesioned core, moreover, levels of TREM2

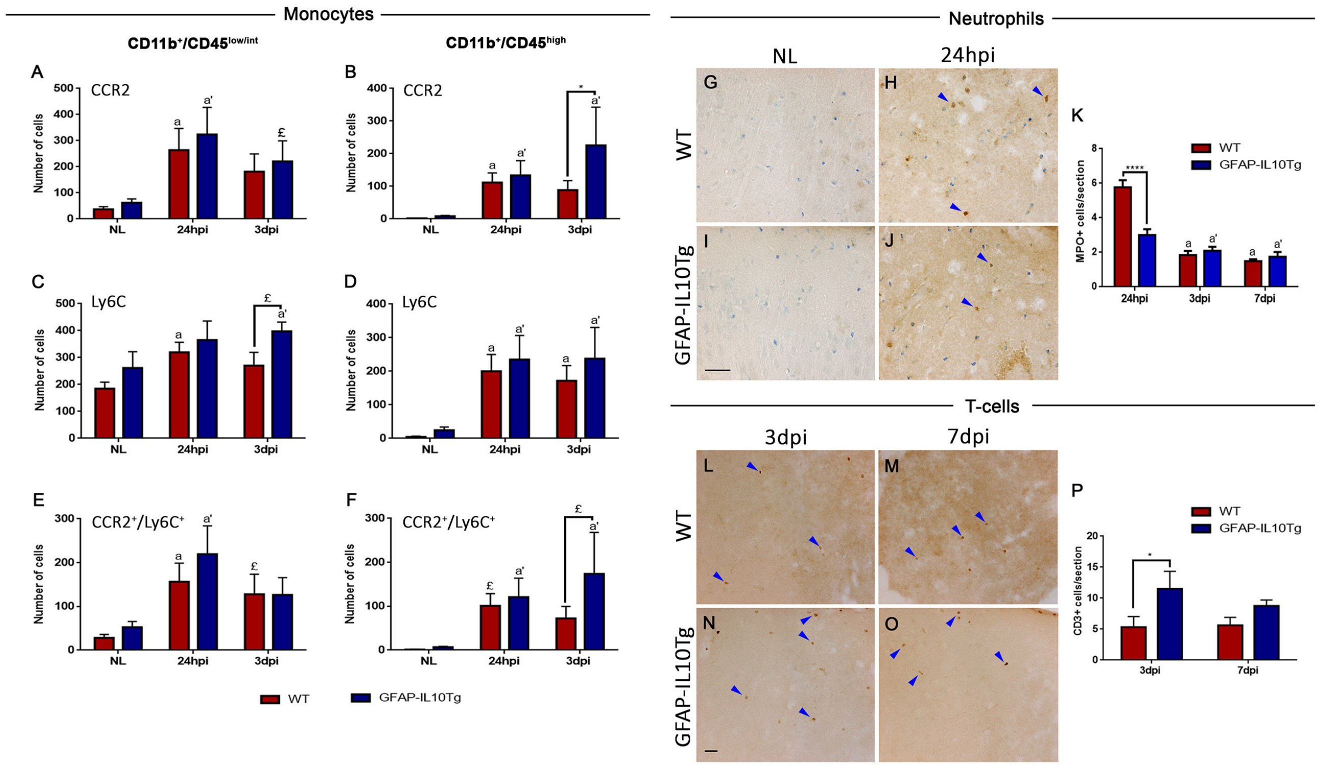

Fig. 9. Peripheral immune cell infiltration. (A~D) Graphs showing the number of CCR2+ and Ly6C+ cells in the microglia (CD11b+/$CD45^{low/int}$) and macrophage (CD11b+/$CD45^{high}$) populations in non-lesioned (NL) and lesioned animals at 24 hpi and 3 dpi in WT and GFAP-IL10Tg mice. (E, F) Graphs showing the quantification of CCR2+/Ly6C+ inflammatory monocytes in non-lesioned (NL) and TBI-lesioned animals at 24 hpi and 3 dpi in WT and GFAP-IL10Tg mice. Inflammatory monocytes exhibited a significant increase in transgenic animals at 3 dpi. In WT animals: "a" indicates significant vs NL and in GFAP-IL10Tg animals: "a'" indicates significant vs NL. (G~J) Representative images showing the number of myeloperoxidase (MPO)+ cells (arrowheads) in the penumbra of TBI-lesioned WT (H) and GFAP-IL10Tg animals (J) at 24 hpi. Toluidine blue staining was used as a nuclei marker. (K) Graph showing the quantification of MPO+cells in WT and GFAP-IL10Tg animals from 24 hpi to 7 dpi. Note that, at 24 hpi, GFAP-IL10Tg animals presented a significantly lower number of MPO+ cells than did WT. In WT animals: "a" indicates significant vs 24 hpi. In GFAP-IL10Tg animals: "a'" indicates significant vs 24 hpi. (L~O) Representative images showing the number of CD3+ T lymphocytes (arrowheads) in the penumbra of both WT (L, M) and GFAP-IL10Tg animals (N, O) at 3 dpi and 7 dpi. (P) Graph showing the quantification of CD3+ T lymphocytes in WT and GFAP-IL10Tg animals at 3 dpi and 7 dpi. Note that,GFAP-IL10Tg presented a higher number of CD3+ lymphocytes than did WT at 3 dpi. All values are represented as mean±SEM ($^{£}p\leq0.1$, $^{*}p\leq0.05$, $^{****}p\leq0.0001$). Scale bar=30 μm.

continued increasing until 7 dpi only in GFAP-IL10Tg mice (Fig. 8Q). TREM2+ cells displayed amoeboid morphology principally, but also some scattered ramified TREM2+ cells were observed (Fig. 8L, M, O, P).

Peripheral immune cells

The putative influence of IL-10 on the infiltration of peripheral immune cells with a key role in the control of TBI was assessed by flow cytometry and immunohistochemistry. To assess monocytes/macrophages migration, CCR2-Ly6C expression was analyzed through flow cytometry, whereas for neutrophils and T cells, the immunohistochemistry against myeloperoxidase (MPO) and CD3, respectively, was used (Fig. 9).

Monocytes/macrophages

As already commented above, the population of CD11b+/CD-45^{high} cells was augmented in GFAP-IL10Tg animals (Fig. 4D). This population, among macrophages and highly activated microglia, may include monocytes, a cell population closely related to TBI progression. Therefore, a putative effect of IL-10 production on monocyte infiltration was studied in more detail using CCR2 and Ly6C by flow cytometry. In NL conditions, a low amount of CCR2+ cells and Ly6C+ cells in the CD11b+/$CD45^{high}$ population was detected in both experimental groups (Fig. 9B, D). After TBI, both WT and GFAP-IL10Tg animals showed an increase in the number of CCR2+, Ly6C+ and CCR2+/Ly6C+ cells in the CD11b+/$CD45^{high}$ (Fig. 9B, D, F) population. This increase followed a similar dynamic in both groups, increasing at 24 hpi and remaining without significant modifications at 3 dpi. Neverthe-

 https://doi.org/10.5607/en21035

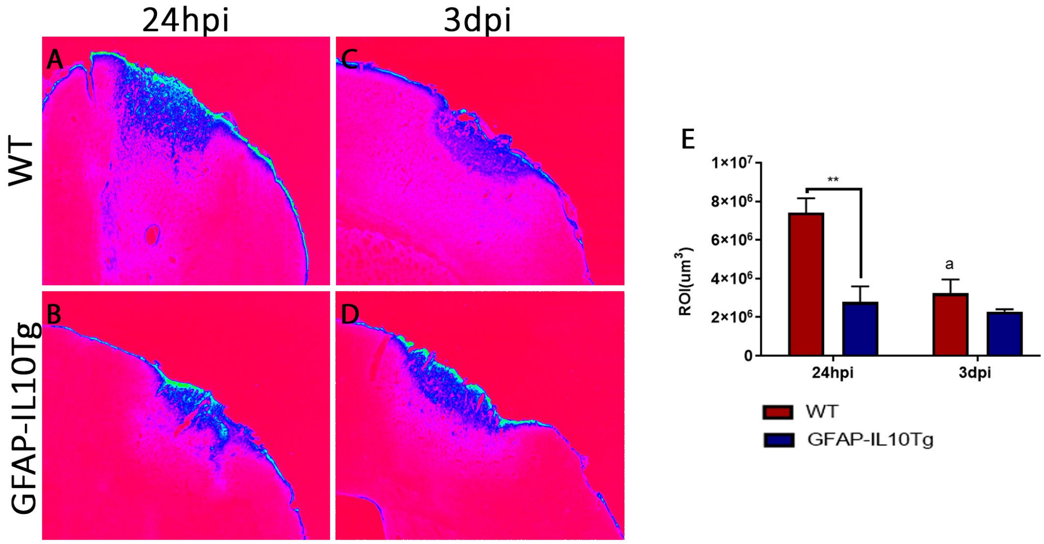

Fig. 10. IgG immunohistochemistry. (A~D) Representative images showing IgG immunostaining (pseudo-color technique modified by LUT filter in Image J software) representing BBB leakage in WT (A, C) and GFAP-IL10Tg animals (B, D) at 24 hpi and 3 dpi. Blue staining represented IgG staining, whereas a red color represented a non-stained area. (E) Graph showing the quantification of volume (ROI) occupied by the IgG staining in WT and GFAP-IL10Tg animals at 24 hpi and 3 dpi. Note that transgenic animals presented a significantly lower lgG extravasation, in comparison to WT at 24 hpi. All values are represented as mean±SEM (**p≤0.01). In WT animals, "a" indicates significant vs 24 hpi.

less, when compared between genotypes, we observed a significantly higher number of CCR2+ and CCR2+/Ly6C+ cells in the CD11b+/CD45^{high} population of transgenic animals (Fig. 9B, F).

Noticeably, some CCR2+, Ly6C+ and double CCR2+/Ly6C+ cells also appeared in the population of CD11b+/CD45$^{low/int}$ microglia after TBI, whose numbers were higher in the case of Ly6C in transgenic mice (Fig. 9A, C, E).

Neutrophil recruitment

Regarding neutrophil infiltration, no MPO+ cells were observed in NL WT or NL GFAP-IL10Tg animals (Fig. 9G, I). After TBI, MPO+ cells appeared in both WT and GFAP-IL10Tg animals at 24 hpi and decreased significantly at 3 dpi. The number of MPO+ was significantly lower at 24 hpi in transgenic mice (Fig. 9H, J, K).

Lymphocyte infiltration

In terms of T cells, no CD3+ cells were detected in either NL WT or NL GFAP-IL10Tg animals. After TBI, CD3+ T lymphocytes appeared accumulated in the PLP in both genotypes at 3 dpi and remained stable at 7 dpi (Fig. 9L~O). A two-fold increase in the total number of CD3+ cells was found at 3 dpi in GFAP-IL10Tg, when compared with WT (Fig. 9P).

Blood brain barrier permeability

To evaluate the possibility that the modifications in the infiltration of peripheral immune cells observed in GFAP-IL10Tg animals were linked to modifications in the permeability of the blood brain barrier (BBB), detection of the immunoglobulin (IgG), indicative of leakage, was used (Fig. 10). IgG immunostaining was not detected in NL WT or NL GFAP-IL10Tg animals (data not shown). After TBI, in WT animals, a strong IgG staining was observed within the lesioned core and diffused into the PLP area at 24 hpi followed by a significant decrease at 3 dpi (Fig. 10A,C, E). In contrast to WT, the IgG staining in GFAP-IL10Tg animals was remarkably low at 24 hpi and remained unaltered at 3 dpi (Fig. 10B, D, E).

Cytokines/chemokines profile

After this, we address whether all modifications observed in transgenic animals were due to changes in the profile of the cytokine/chemokine. We specifically analyzed the expression of key cytokines linked to TBI, such as IL-1β, IL-10, TGF-β1, and chemokines related to the recruitment of neutrophils and monocytes, such as CXCL1 and CCL2, respectively. Our results demonstrated a significant increase in the expression of IL-1β a few hours after injury (4 hpi) in both WT and GFAP-IL10Tg that remained without significant modifications in WT, but returned to basal levels at 24 hpi in transgenic animals (Fig. 11A). Noticeably, GFAP-IL10Tg animals showed a significant decrease of IL-1β at 24 hpi, in comparison to WT (Fig. 11A). Regarding IL-10, whereas in WT animals the significant increase was not observed until 24 hpi, levels in transgenic animals were already higher at earlier time-points (4

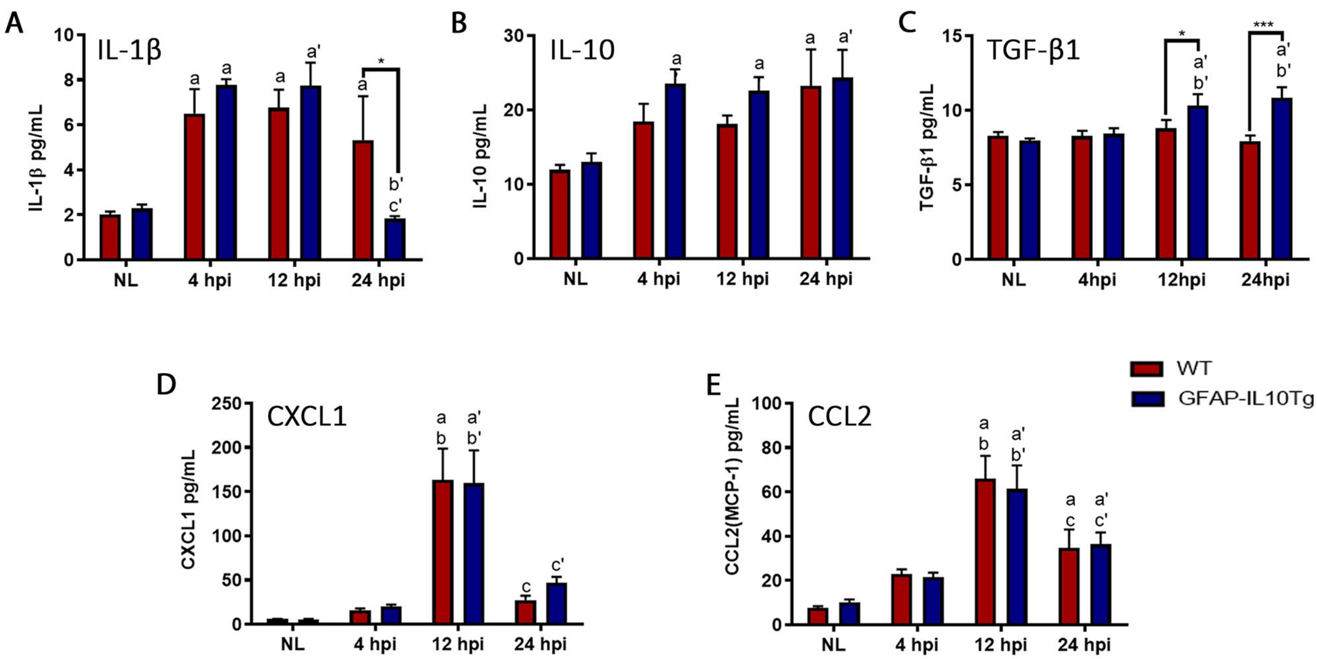

Fig. 11. Cytokine/chemokine expression. Graphs showing the temporal expression of IL-1β (A), IL-10 (B), TGF-β1 (C), CXCL1 (D) and CCL2 (E) in non-lesioned (NL) and TBI-lesioned animals from 4 hpi to 24 hpi in both WT and GFAP-IL10Tg animals. Note the lower levels of IL-1β and the higher levels of TGF-β1 observed in GFAP-IL10Tg mice at 12 hpi and 24 hpi. All values are represented as mean±SEM (*$p\leq0.05$, ***$p\leq0.001$). In WT animals: "a" indicates significant vs NL, "b" indicates significant vs 4 hpi, "c" indicates significant vs 12 hpi. In GFAP-IL10Tg animals: "a'" indicates significant vs NL, "b'" indicates significant vs 4 hpi, "c'" indicates significant vs 12 hpi.

hpi and 12 hpi) (Fig. 11B). In addition, a remarkable up-regulation in the level of TGF-β1 was observed at 12 hpi and 24 hpi only in transgenic animals (Fig. 11C). Both CXCL1 and CCL2 showed an important increase at 12 hpi, decreasing thereafter at 24 hpi in both WT and GFAP-IL10Tg animals, without significant differences between genotypes at any time-point analyzed (Fig. 11D, E). TNF-α was not detected with this technique in any genotype at any time-point analyzed.

IL-10 receptor (IL-10R) staining

Finally, in order to study the target cells responding to the production of IL-10, the cells carrying the IL-10 receptor (IL-10R) were analyzed in both basal conditions and after TBI, using double immunofluorescence. In NL conditions, both WT and GFAP-IL10Tg animals showed expression of IL-10R in a few GFAP+ cells randomly distributed along the cortex (Fig. 12A~F). After TBI, IL-10R+/GFAP+ cells increased in both WT and GFAP-IL10Tg animals and were specifically located in the PLP area (just surrounding the lesion cavity) (Fig. 12G~L). No detectable differences in the number of double-positive cells were found between genotypes. Additionally, some IL-10R+ cells morphologically identified as neurons were observed in the PLP area in both genotypes without differences among them (data not shown).

DISCUSSION

In this study, have shown that astrocyte-targeted local production of IL-10 induces a decrease of the neuronal degeneration associated with TBI. This neuro-protection correlates with an increase in the microglia/macrophage cell density with an up-regulated phagocytic phenotype. Moreover, local IL-10 production reduces BBB leakage, inducing lower neutrophil recruitment but up-regulating the infiltration of monocyte/macrophages and T lymphocytes to the site of injury. All of these changes are associated with significant modifications in the expression of cytokines, including a decrease of IL-1β and an increase in TGF-β1.

Reduction in neuronal degeneration in GFAP-IL10Tg mice after TBI

Neuro-degeneration is the principal cause of disability after TBI and is the major determinant of long-term outcomes. The initial primary injury causes direct mechanical damage to the brain tissue and neurons, whereas secondary injury is the result of different molecular, cellular and physiological processes initiated following this primary insult. Secondary injury is mediated by several factors, including free radicals production, excitotoxicity as well as the neuro-inflammatory response linked to TBI [36].

 https://doi.org/10.5607/en21035

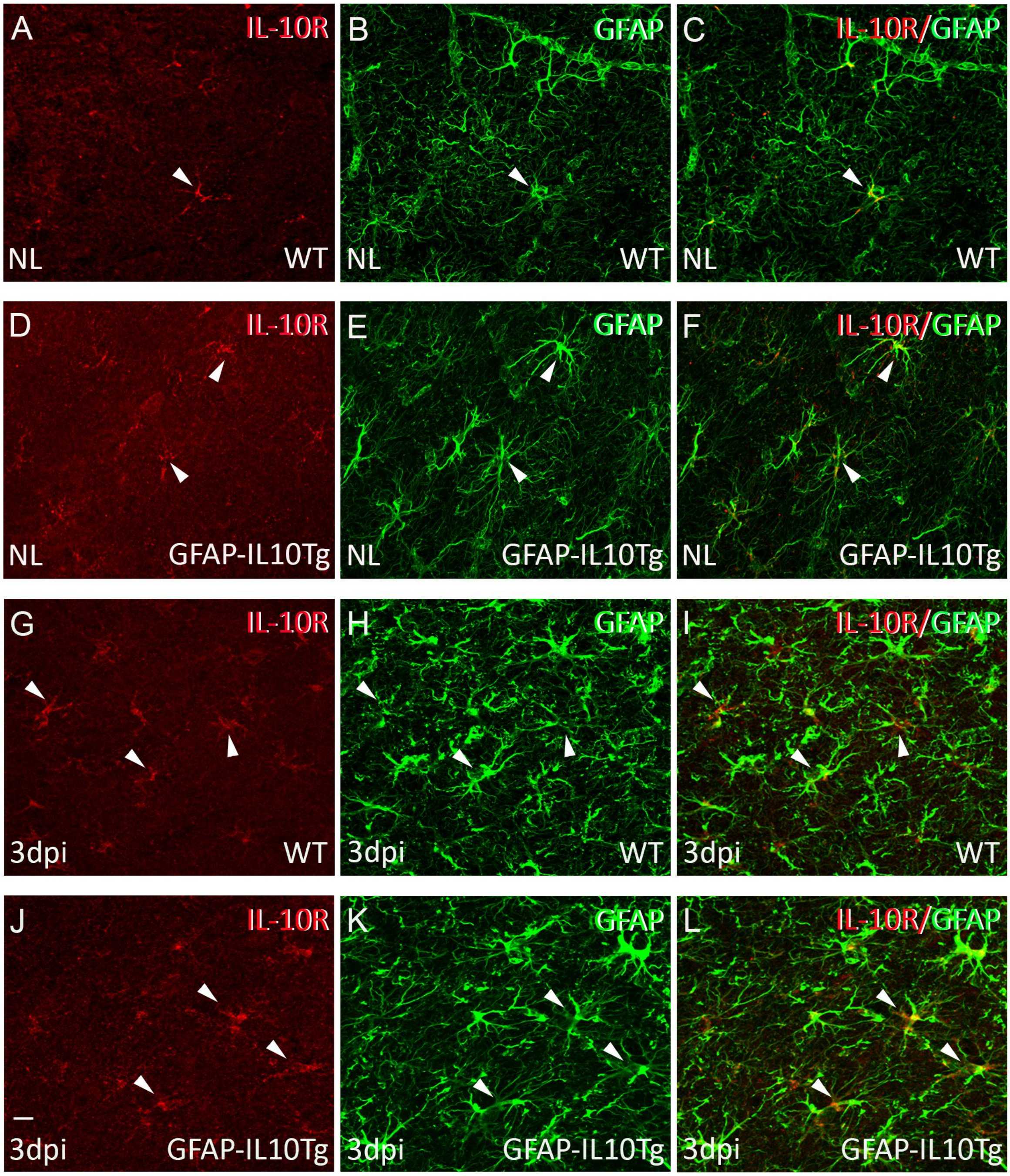

Fig. 12. IL-10R expression. Representative images showing the double immunofluorescence combining IL-10R (red) and GFAP (green) in non-lesioned (NL) (A~F) and TBI-lesioned animals at 3 dpi (G~L). Note that a major part of IL-10R+ cells showed co-localization (yellow) with GFAP in both NL and after TBI in both genotypes (arrowheads). Scale bar=10 μm.

In agreement with previous studies [37, 38], in this study injured neurons appeared in the ipsilateral cortex surrounding the impact site by 1 and 3 days after injury. The neuro-protective effect of IL-10 was observed following TBI with a significant decrease in the number of FJ-B+ degenerating neurons at early time-points. Similarly, some studies have reported the anti-inflammatory and neuro-protective properties of systemic administration of IL-10 after TBI [26] and stroke [22], as well as the protective effects of astrocyte-targeted production of IL-10 after facial nerve axotomy [29] and perforant pathway transection [30]. It has been extensively demonstrated that after TBI the neuro-protective effect of IL-10 is exerted via suppressing the expression of various pro-inflammatory cytokines, such as TNF-α, IL-1β, IL-2, IL-6, MIP-2 and MCP-1(CCL2) [26, 39]. In agreement, in our study, a decrease in the amount of IL-1β is observed in GFAP-IL10Tg animals at those time-points where the neuro-protection is reported. Moreover, to our knowledge, this is the first study to report beneficial effects of IL-10 after TBI when produced locally in the CNS.

Whether this effect is directly on neurons, indirect on other CNS cells, or is the consequence of both effects together is a difficult statement to answer. On one hand, we observed IL-10R+ neurons in the area surrounding the lesion cavity, the same area where degenerating FJ-B+ neurons were localized, pointing to a putative direct protective effect over neurons, as described in other injury models, by promoting neuronal survival [40] and/or preventing neuronal death [41]. However, also, GFAP+ astrocytes located in the penumbra of the lesion have been detected, and transgenic animals presented important modifications in the microglial reactivity and peripheral immune cell infiltration, making it impossible to exclude the possibility of an indirect neuro-protective effect of IL-10 through the action on astrocytes. We will discuss these issues in detail in the following paragraphs.

Microglia/macrophages in GFAP-IL10Tg animals showed an increase in numbers and more phagocytic phenotype

Microglia/macrophage activation is a common feature of the neuro-inflammatory response associated with most of neurological pathologies, including TBI. Microglial activation occurs early after TBI in both experimental animal models and human patients and can be activated chronically for years [42-44]. The acute response of microglia to TBI is to migrate to the site of injury to mitigate inflammation by eradicating toxic substances and removing/phagocytosing death cells from the environment, to restore the normal brain environment and permit tissue repair. In addition, activated microglia produce and release pro-inflammatory cytokines such as TNF-α, IL-1β, CCL2, CXCL1, reactive oxygen species (ROS) and reactive nitrogen species (RNS), which are deleterious to neurons and perpetuate tissue damage [45-49].

Our results showed a significant increase in microglia/macrophage cell density after TBI in both WT and GFAP-IL10Tg animals, but being higher in transgenic animals, especially at 3 dpi. Microglial proliferation has been proposed as being the main possible mechanism mediating microglia/macrophage expansion after TBI [50, 51]. However, the total number of mitotic cells in GFAP-IL10Tg animals decreased in our study, correlating with the lower-fold increase reported in transgenic mice in terms of Iba1 and Pu.1. These results pointed to IL-10 as an inhibiting factor for the microglial proliferation phenomenon, as we already reported in our previous results [30]. Although initially, it seems paradoxical, as GFAP-IL10Tg showed a higher number of microglia/macrophage cells, it is important to take into account here that the amount of microglial cells in NL conditions is already higher in transgenic animals than in WT. The fact that we did not detect IL-10R expression on microglia/macrophage cells after TBI, together with previous studies *in vitro* [52, 53] or *in vivo* [30] showing no direct effects of IL-10 on microglial proliferation, suggest that the modification in microglial proliferation might be an indirect effect mediated by IL-10 over degenerating neurons and/or astrocytes, the principal cells expressing the IL-10R.

In addition to the proliferation process, local production of IL-10 may influence the extension of microglial survival and/or monocytes/macrophages recruitment and could be another possibility to explain the expansion of microglia/macrophage cell density induced by IL-10. Inflammatory monocytes/macrophages have been described as the major recruited peripheral immune cells between 3 and 5 days after TBI [54-57]. In concordance, our results clearly showed the presence of CCR2+/Ly6C+ inflammatory monocytes within the CD11b+/CD45^{high} cell population of both experimental groups. The number of recruited inflammatory monocytes was higher in GFAP-IL10Tg animals at 3 dpi, the time-point in which maximal differences in microglia/macrophage cell density were detected between WT and transgenic mice, suggesting that IL-10 is influencing the recruitment of peripheral inflammatory monocytes. We did not detect differences in the amount of the CCL2 level, the principal chemokine involved in monocyte recruitment, between genotypes, at least at the early time-points data analyzed, suggesting that other mechanisms rather than chemokines impact on monocyte recruitment by IL-10. As we comment in the following paragraphs, modifications in the BBB could be the reason.

In addition to modifications in cell number, we reported lower Iba1 levels in activated microglia of GFAP-IL10Tg at later time-points, supporting the previous reports that described a down-regulatory effect of IL-10 on microglial activation [14, 53]. However, these transgenic activated microglia are also characterized by higher expression of both CD68 and TREM2 markers usually linked with phagocytosis [58], particularly in the lesioned core at early time-points. As already commented, one of the main functions of acutely activated microglia is to eliminate dead cells from the injury site to permit tissue regeneration and repair. Thus, the higher number of CD68+ and TREM2+ microglia detected on GFAP-IL10Tg mice could be related to more rapid and efficient phagocytosis of cellular debris, which can lead to the reduction in neuro-degeneration observed in these animals.

Decreased blood brain barrier permeability reduces neutrophil infiltration but increases T lymphocyte

recruitment in GFAP-IL10Tg mice

Blood brain barrier (BBB) leakage has been demonstrated during the acute phase of several experimental animal models of TBI [59-62]. The opening of BBB occurs around 1 hour post injury and lasts for a longer time at 4, and even 7 days post-TBI [59, 60]. Acute BBB breakdown after an injury is concomitant with a rapid neutrophil infiltration into the injured parenchyma, peaking between 24 hpi and 3 dpi, which could greatly aggregate the secondary tissue damage by secreting and releasing neurotoxic factors [56, 63]. In our study, vascular damage occurred in both WT and GFAP-IL10Tg animals at 24 hpi and 3 dpi. Interestingly, the permeable abnormalities of BBB in GFAP-IL10Tg animals are strongly attenuated at 24 hpi, accompanied by a significant decrease in neutrophil recruitment into the injured parenchyma. Infiltration of neutrophils is one of the first events in the neuro-inflammatory cascade, turned on after TBI [56, 63]. Detrimental consequences have been associated with neutrophil infiltration, ranging from the direct toxic effects on neurons of matrix metallo-proteinases and reactive oxygen species to edema and cellular metabolic stress resulting from the increase of vascular permeability [64]. Therapeutic neutrophil depletion demonstrated reduced brain tissue loss, reduced microglial activation and cell death [65], as well as a benefit in neurological outcome [66]. These studies lead us to speculate that local production of IL-10 is modifying blood brain permeability, at early 24 hpi, inducing lower recruitment of neutrophils that leads to lower neuronal degeneration.

Besides the reduction in BBB leakage and neutrophil migration, GFAP-IL10Tg animals showed a higher number of infiltrated CD3+ T cells. Similar results were reported using the same transgenic animal after facial nerve axotomy [29] and perforant pathway transection [30]. Recruitment of T cells after TBI appears to occur together with monocytes/macrophages during acute and chronic phases [67, 68]. However, the exact role played by lymphocytes in the context of TBI was poorly understood, as controversial results were obtained in different animal models. Some reports showed that T cells exacerbated the post-traumatic tissue damage injury [69], whereas other studies reported no differences between wild-type and Rag-/- mice (which lack lymphocyte responses) in terms of injury severity and neurologic impairment after a closed head injury [70]. According to our results, GFAP-IL10Tg mice have more T cells together with neuro-protective effects. This protective effect could be related to differences in the phenotype of T cells. A positive correlation between higher T-regulatory cells (T-regs) in the blood and a better clinical outcome has been reported in TBI patients [71]. Moreover, depletion of T-regs after TBI leads to aggravating motor deficits [72]. Thus, a detailed study of the different T cell subsets, especially T-regs, in the context of the GFAP-IL10Tg animals, is necessary to clearly understand the role of IL-10 in the neuro-immune response associated with TBI.

Astrocytes and degenerating neurons are the principal cell types expressing the IL-10R

Finally, we wish to explore the cells responsible for IL-10R. Our results clearly demonstrated that astrocytes and neurons located in the penumbra area are the principal cells expressing IL-10R after TBI. In agreement with this, previous reports *in vitro* and *in vivo* described the expression of IL-10R in astrocytes [13-15, 27] and neurons [17, 27] under physiological and pathological conditions. These results indicate that all of the modifications observed in the microglial activation pattern and BBB leakage may be related to the indirect effects of IL-10 on astrocytes and/or degenerating neurons located in the penumbra.

Indeed, the dynamic interaction between microglia and astrocytes has been described in some studies to be mediated by cytokines such as TGF-β [14, 73, 74]. Norden and colleagues demonstrated that astrocytes stimulated by IL-10 secrete TGF-β and that this TGF-β down-regulates LPS-activated microglial activation associated with a reduction in pro-inflammatory cytokines such as IL-1β, IL-6, CCL2, TNF-α [14]. Thus, it is plausible that IL-10 signaling acts directly on astrocytes, which produces and secretes high levels of TGF-β, and this cytokine modulates microglia activation. Nevertheless, further studies are mandatory to analyze astrocyte-microglia communication molecules specifically after TBI, to decipher the specific role exerted by IL-10.

CONCLUSION

In this study, we show that IL-10 exerted a neuro-protective effect at early time-points after TBI. This effect could be mediated by a direct effect on neurons located in the penumbra carrying the IL-10R and by indirect effects derived from the effects exerted on astrocytes, the other cell-type expressing the receptor. IL-10R signaling in astrocytes involves an increase in the secretion of TGF-β1, an anti-inflammatory communicator molecule between microglia and astrocytes, which attenuates microglial activation and pro-inflammatory cytokine production (IL-1β) but upregulates the microglial phagocytic phenotype, producing a better elimination of cellular debris. In addition, IL-10 production within the CNS reduces BBB leakage and neutrophil migration as well as promoting monocyte/macrophage and T lymphocyte recruitment, shifting to an anti-inflammatory and protective immune inflammatory response.

ACKNOWLEDGEMENTS

The authors would like to thank Miguel Angel Martil and Isabella Appiah for their outstanding laboratory technical assistance and Mireia Recasens for her help on confocal microscopy. This work was supported by the Spanish Ministry of Economy and Competitiveness (BFU2104-55459 and BFU2017-87843-R) to BC.

REFERENCES

1. Greve MW, Zink BJ (2009) Pathophysiology of traumatic brain injury. Mt Sinai J Med 76:97-104.
2. Ghajar J (2000) Traumatic brain injury. Lancet 356:923-929.
3. Thornhill S, Teasdale GM, Murray GD, McEwen J, Roy CW, Penny KI (2000) Disability in young people and adults one year after head injury: prospective cohort study. BMJ 320:1631-1635.
4. Masel BE, DeWitt DS (2010) Traumatic brain injury: a disease process, not an event. J Neurotrauma 27:1529-1540.
5. Cederberg D, Siesjö P (2010) What has inflammation to do with traumatic brain injury? Childs Nerv Syst 26:221-226.
6. Cole PJ (1986) Inflammation: a two-edged sword--the model of bronchiectasis. Eur J Respir Dis Suppl 147:6-15.
7. Doyle KP, Buckwalter MS (2012) The double-edged sword of inflammation after stroke: what sharpens each edge? Ann Neurol 71:729-731.
8. Cerecedo-López CD, Kim-Lee JH, Hernandez D, Acosta SA, Borlongan CV (2014) Insulin-associated neuroinflammatory pathways as therapeutic targets for traumatic brain injury. Med Hypotheses 82:171-174.
9. Couper KN, Blount DG, Riley EM (2008) IL-10: the master regulator of immunity to infection. J Immunol 180:5771-5777.
10. Moore KW, de Waal Malefyt R, Coffman RL, O'Garra A (2001) Interleukin-10 and the interleukin-10 receptor. Annu Rev Immunol 19:683-765.
11. Hulshof S, Montagne L, De Groot CJ, Van Der Valk P (2002) Cellular localization and expression patterns of interleukin-10, interleukin-4, and their receptors in multiple sclerosis lesions. Glia 38:24-35.
12. Park KW, Lee HG, Jin BK, Lee YB (2007) Interleukin-10 endogenously expressed in microglia prevents lipopolysaccharide-induced neurodegeneration in the rat cerebral cortex in vivo. Exp Mol Med 39:812-819.
13. Ledeboer A, Brevé JJ, Wierinckx A, van der Jagt S, Bristow AF, Leysen JE, Tilders FJ, Van Dam AM (2002) Expression and regulation of interleukin-10 and interleukin-10 receptor in rat astroglial and microglial cells. Eur J Neurosci 16:1175-1185.
14. Norden DM, Fenn AM, Dugan A, Godbout JP (2014) TGFβ produced by IL-10 redirected astrocytes attenuates microglial activation. Glia 62:881-895.
15. Gonzalez P, Burgaya F, Acarin L, Peluffo H, Castellano B, Gonzalez B (2009) Interleukin-10 and interleukin-10 receptor-I are upregulated in glial cells after an excitotoxic injury to the postnatal rat brain. J Neuropathol Exp Neurol 68:391-403.
16. Cannella B, Raine CS (2004) Multiple sclerosis: cytokine receptors on oligodendrocytes predict innate regulation. Ann Neurol 55:46-57.
17. Xin J, Wainwright DA, Mesnard NA, Serpe CJ, Sanders VM, Jones KJ (2011) IL-10 within the CNS is necessary for $CD4^+$ T cells to mediate neuroprotection. Brain Behav Immun 25:820-829.
18. Lodge PA, Sriram S (1996) Regulation of microglial activation by TGF-beta, IL-10, and CSF-1. J Leukoc Biol 60:502-508.
19. Balasingam V, Yong VW (1996) Attenuation of astroglial reactivity by interleukin-10. J Neurosci 16:2945-2955.
20. Bethea JR, Nagashima H, Acosta MC, Briceno C, Gomez F, Marcillo AE, Loor K, Green J, Dietrich WD (1999) Systemically administered interleukin-10 reduces tumor necrosis factor-alpha production and significantly improves functional recovery following traumatic spinal cord injury in rats. J Neurotrauma 16:851-863.
21. Ooboshi H, Ibayashi S, Shichita T, Kumai Y, Takada J, Ago T, Arakawa S, Sugimori H, Kamouchi M, Kitazono T, Iida M (2005) Postischemic gene transfer of interleukin-10 protects against both focal and global brain ischemia. Circulation 111:913-919.
22. Spera PA, Ellison JA, Feuerstein GZ, Barone FC (1998) IL-10 reduces rat brain injury following focal stroke. Neurosci Lett 251:189-192.
23. Brewer KL, Bethea JR, Yezierski RP (1999) Neuroprotective effects of interleukin-10 following excitotoxic spinal cord injury. Exp Neurol 159:484-493.
24. Cua DJ, Hutchins B, LaFace DM, Stohlman SA, Coffman RL (2001) Central nervous system expression of IL-10 inhibits autoimmune encephalomyelitis. J Immunol 166:602-608.
25. Cannella B, Gao YL, Brosnan C, Raine CS (1996) IL-10 fails to abrogate experimental autoimmune encephalomyelitis. J Neurosci Res 45:735-746.
26. Knoblach SM, Faden AI (1998) Interleukin-10 improves out-

come and alters proinflammatory cytokine expression after experimental traumatic brain injury. Exp Neurol 153:143-151.
27. Almolda B, de Labra C, Barrera I, Gruart A, Delgado-Garcia JM, Villacampa N, Vilella A, Hofer MJ, Hidalgo J, Campbell IL, González B, Castellano B (2015) Alterations in microglial phenotype and hippocampal neuronal function in transgenic mice with astrocyte-targeted production of interleukin-10. Brain Behav Immun 45:80-97.
28. Sanchez-Molina P, Almolda B, Benseny-Cases N, González B, Perálvarez-Marín A, Castellano B (2021) Specific microglial phagocytic phenotype and decrease of lipid oxidation in white matter areas during aging: implications of different microenvironments. Neurobiol Aging 105:280-295.
29. Villacampa N, Almolda B, Vilella A, Campbell IL, González B, Castellano B (2015) Astrocyte-targeted production of IL-10 induces changes in microglial reactivity and reduces motor neuron death after facial nerve axotomy. Glia 63:1166-1184.
30. Recasens M, Shrivastava K, Almolda B, González B, Castellano B (2019) Astrocyte-targeted IL-10 production decreases proliferation and induces a downregulation of activated microglia/macrophages after PPT. Glia 67:741-758.
31. Albert-Weissenberger C, Sirén AL (2010) Experimental traumatic brain injury. Exp Transl Stroke Med 2:16.
32. Sirén AL, Radyushkin K, Boretius S, Kämmer D, Riechers CC, Natt O, Sargin D, Watanabe T, Sperling S, Michaelis T, Price J, Meyer B, Frahm J, Ehrenreich H (2006) Global brain atrophy after unilateral parietal lesion and its prevention by erythropoietin. Brain 129(Pt 2):480-489.
33. Perego C, Fumagalli S, De Simoni MG (2011) Temporal pattern of expression and colocalization of microglia/macrophage phenotype markers following brain ischemic injury in mice. J Neuroinflammation 8:174.
34. Almolda B, Costa M, Montoya M, González B, Castellano B (2009) CD4 microglial expression correlates with spontaneous clinical improvement in the acute Lewis rat EAE model. J Neuroimmunol 209:65-80.
35. Gómez-Nicola D, Fransen NL, Suzzi S, Perry VH (2013) Regulation of microglial proliferation during chronic neurodegeneration. J Neurosci 33(6):2481-2493.
36. Jassam YN, Izzy S, Whalen M, McGavern DB, El Khoury J (2017) Neuroimmunology of traumatic brain injury: time for a paradigm shift. Neuron 95:1246-1265.
37. Sato M, Chang E, Igarashi T, Noble LJ (2001) Neuronal injury and loss after traumatic brain injury: time course and regional variability. Brain Res 917:45-54.
38. Conti AC, Raghupathi R, Trojanowski JQ, McIntosh TK (1998) Experimental brain injury induces regionally distinct apoptosis during the acute and delayed post-traumatic period. J Neurosci 18:5663-5672.
39. Chen X, Duan XS, Xu LJ, Zhao JJ, She ZF, Chen WW, Zheng ZJ, Jiang GD (2014) Interleukin-10 mediates the neuroprotection of hyperbaric oxygen therapy against traumatic brain injury in mice. Neuroscience 266:235-243.
40. Zhou Z, Peng X, Insolera R, Fink DJ, Mata M (2009) IL-10 promotes neuronal survival following spinal cord injury. Exp Neurol 220:183-190.
41. Sharma S, Yang B, Xi X, Grotta JC, Aronowski J, Savitz SI (2011) IL-10 directly protects cortical neurons by activating PI-3 kinase and STAT-3 pathways. Brain Res 1373:189-194.
42. Loane DJ, Kumar A, Stoica BA, Cabatbat R, Faden AI (2014) Progressive neurodegeneration after experimental brain trauma: association with chronic microglial activation. J Neuropathol Exp Neurol 73:14-29.
43. Ramlackhansingh AF, Brooks DJ, Greenwood RJ, Bose SK, Turkheimer FE, Kinnunen KM, Gentleman S, Heckemann RA, Gunanayagam K, Gelosa G, Sharp DJ (2011) Inflammation after trauma: microglial activation and traumatic brain injury. Ann Neurol 70:374-383.
44. Johnson VE, Stewart JE, Begbie FD, Trojanowski JQ, Smith DH, Stewart W (2013) Inflammation and white matter degeneration persist for years after a single traumatic brain injury. Brain 136(Pt 1):28-42.
45. Shohami E, Gallily R, Mechoulam R, Bass R, Ben-Hur T (1997) Cytokine production in the brain following closed head injury: dexanabinol (HU-211) is a novel TNF-alpha inhibitor and an effective neuroprotectant. J Neuroimmunol 72:169-177.
46. Allan SM, Rothwell NJ (2001) Cytokines and acute neurodegeneration. Nat Rev Neurosci 2:734-744.
47. Chao CC, Hu S, Ehrlich L, Peterson PK (1995) Interleukin-1 and tumor necrosis factor-alpha synergistically mediate neurotoxicity: involvement of nitric oxide and of N-methyl-D-aspartate receptors. Brain Behav Immun 9:355-365.
48. Gyoneva S, Ransohoff RM (2015) Inflammatory reaction after traumatic brain injury: therapeutic potential of targeting cell-cell communication by chemokines. Trends Pharmacol Sci 36:471-480.
49. Harting MT, Jimenez F, Adams SD, Mercer DW, Cox CS Jr (2008) Acute, regional inflammatory response after traumatic brain injury: implications for cellular therapy. Surgery 144:803-813.

50. Susarla BT, Villapol S, Yi JH, Geller HM, Symes AJ (2014) Temporal patterns of cortical proliferation of glial cell populations after traumatic brain injury in mice. ASN Neuro 6:159-170.
51. Tatsumi K, Haga S, Matsuyoshi H, Inoue M, Manabe T, Makinodan M, Wanaka A (2005) Characterization of cells with proliferative activity after a brain injury. Neurochem Int 46:381-389.
52. Strle K, Zhou JH, Broussard SR, Venters HD, Johnson RW, Freund GG, Dantzer R, Kelley KW (2002) IL-10 promotes survival of microglia without activating Akt. J Neuroimmunol 122:9-19.
53. Sawada M, Suzumura A, Hosoya H, Marunouchi T, Nagatsu T (1999) Interleukin-10 inhibits both production of cytokines and expression of cytokine receptors in microglia. J Neurochem 72:1466-1471.
54. Rhodes J (2011) Peripheral immune cells in the pathology of traumatic brain injury? Curr Opin Crit Care 17:122-130.
55. Holmin S, Mathiesen T, Shetye J, Biberfeld P (1995) Intracerebral inflammatory response to experimental brain contusion. Acta Neurochir (Wien) 132:110-119.
56. Soares HD, Hicks RR, Smith D, McIntosh TK (1995) Inflammatory leukocytic recruitment and diffuse neuronal degeneration are separate pathological processes resulting from traumatic brain injury. J Neurosci 15:8223-8233.
57. Hsieh CL, Kim CC, Ryba BE, Niemi EC, Bando JK, Locksley RM, Liu J, Nakamura MC, Seaman WE (2013) Traumatic brain injury induces macrophage subsets in the brain. Eur J Immunol 43:2010-2022.
58. Neumann H, Kotter MR, Franklin RJ (2009) Debris clearance by microglia: an essential link between degeneration and regeneration. Brain 132(Pt 2):288-295.
59. Habgood MD, Bye N, Dziegielewska KM, Ek CJ, Lane MA, Potter A, Morganti-Kossmann C, Saunders NR (2007) Changes in blood-brain barrier permeability to large and small molecules following traumatic brain injury in mice. Eur J Neurosci 25:231-238.
60. Lotocki G, de Rivero Vaccari JP, Perez ER, Sanchez-Molano J, Furones-Alonso O, Bramlett HM, Dietrich WD (2009) Alterations in blood-brain barrier permeability to large and small molecules and leukocyte accumulation after traumatic brain injury: effects of post-traumatic hypothermia. J Neurotrauma 26:1123-1134.
61. Dietrich WD, Alonso O, Halley M (1994) Early microvascular and neuronal consequences of traumatic brain injury: a light and electron microscopic study in rats. J Neurotrauma 11:289-301.
62. Povlishock JT, Becker DP, Sullivan HG, Miller JD (1978) Vascular permeability alterations to horseradish peroxidase in experimental brain injury. Brain Res 153:223-239.
63. Liu YW, Li S, Dai SS (2018) Neutrophils in traumatic brain injury (TBI): friend or foe? J Neuroinflammation 15:146.
64. Lindbom L (2003) Regulation of vascular permeability by neutrophils in acute inflammation. Chem Immunol Allergy 83:146-166.
65. Kenne E, Erlandsson A, Lindbom L, Hillered L, Clausen F (2012) Neutrophil depletion reduces edema formation and tissue loss following traumatic brain injury in mice. J Neuroinflammation 9:17.
66. Bao F, Shultz SR, Hepburn JD, Omana V, Weaver LC, Cain DP, Brown A (2012) A CD11d monoclonal antibody treatment reduces tissue injury and improves neurological outcome after fluid percussion brain injury in rats. J Neurotrauma 29:2375-2392.
67. Timaru-Kast R, Luh C, Gotthardt P, Huang C, Schäfer MK, Engelhard K, Thal SC (2012) Influence of age on brain edema formation, secondary brain damage and inflammatory response after brain trauma in mice. PLoS One 7:e43829.
68. Ndode-Ekane XE, Matthiesen L, Bañuelos-Cabrera I, Palminha CAP, Pitkänen A (2018) T-cell infiltration into the perilesional cortex is long-lasting and associates with poor somatomotor recovery after experimental traumatic brain injury. Restor Neurol Neurosci 36:485-501.
69. Clausen F, Lorant T, Lewén A, Hillered L (2007) T lymphocyte trafficking: a novel target for neuroprotection in traumatic brain injury. J Neurotrauma 24:1295-1307.
70. Weckbach S, Neher M, Losacco JT, Bolden AL, Kulik L, Flierl MA, Bell SE, Holers VM, Stahel PF (2012) Challenging the role of adaptive immunity in neurotrauma: Rag1(-/-) mice lacking mature B and T cells do not show neuroprotection after closed head injury. J Neurotrauma 29:1233-1242.
71. Li M, Lin YP, Chen JL, Li H, Jiang RC, Zhang JN (2015) Role of regulatory T cell in clinical outcome of traumatic brain injury. Chin Med J (Engl) 128:1072-1078.
72. Krämer TJ, Hack N, Brühl TJ, Menzel L, Hummel R, Griemert EV, Klein M, Thal SC, Bopp T, Schäfer MKE (2019) Depletion of regulatory T cells increases T cell brain infiltration, reactive astrogliosis, and interferon-γ gene expression in acute experimental traumatic brain injury. J Neuroinflammation 16:163. Erratum in: J Neuroinflammation (2019) 16:176.
73. Abutbul S, Shapiro J, Szaingurten-Solodkin I, Levy N, Carmy Y, Baron R, Jung S, Monsonego A (2012) TGF-β signaling

through SMAD2/3 induces the quiescent microglial phenotype within the CNS environment. Glia 60:1160-1171.
74. Schilling T, Nitsch R, Heinemann U, Haas D, Eder C (2001) Astrocyte-released cytokines induce ramification and outward K^+ channel expression in microglia via distinct signalling pathways. Eur J Neurosci 14:463-473.